

SOLVING OPTIMAL CONTROL OF RIGID-BODY DYNAMICS WITH COLLISIONS USING THE HYBRID MINIMUM PRINCIPLE

WEI HU*, JIHAO LONG†, YAOHUA ZANG‡, WEINAN E§, AND JIEQUN HAN¶

Abstract. Collisions are common in many dynamical systems with real applications. They can be formulated as hybrid dynamical systems with discontinuities automatically triggered when states transverse certain manifolds. We present an algorithm for the optimal control problem of such hybrid dynamical systems, based on solving the equations derived from the hybrid minimum principle (HMP). The algorithm is an iterative scheme following the spirit of the method of successive approximations, and it is robust to undesired collisions observed in the initial guesses. We carefully analyze and address several numerical challenges introduced by the discontinuities. The algorithm is tested on disc collision problems whose optimal solutions exhibit one or multiple collisions. Linear convergence in terms of the iteration steps and asymptotic first-order accuracy in terms of time discretization are observed when the algorithm is implemented with the forward-Euler scheme. The numerical results demonstrate that the proposed algorithm has better accuracy and convergence than direct methods based on gradient descent. The algorithm is also simpler, more accurate, and more stable than a deep reinforcement learning method.

Key words. optimal control, hybrid minimum principle, discontinuous system, rigid-body collision, Pontryagin's minimum principle

1. Introduction. Discontinuities are ubiquitous in dynamical systems governing many applications, *e.g.* robotics. They can happen either internally as an intrinsic property of the dynamical system or be triggered by external control signals. These mostly smooth systems with the presence of discrete discontinuous phenomena are called hybrid systems. They can be classified according to the different kinds of hybrid phenomena present in the system [8, 9].

In this paper, we study the optimal control of dynamical systems with discrete discontinuities and a Bolza-type objective. Our interest lies in those discontinuities that are jumps of the state variables and are triggered automatically when the states transverse certain manifolds (jumping manifolds). These discontinuities are called *autonomous state jumps*. Rigid body collisions are models for these discontinuities, which are very common in robotics.

Another type of hybrid dynamical system that is widely studied in the literature is called *controlled hybrid system*, *i.e.* when and how the discontinuities affect the system are directly controlled by extra control variables. Such hybrid phenomena are found in many applications such as impulsive control of satellite rendezvous [10], Chua's circuit [22], hybrid vehicle [27, 7]. Most strategies for solving the optimal control problem of the hybrid system decouple the continuous control and the discrete control, including the switching times, switching sequence, jump magnitudes, *etc.* For a comprehensive review that focuses on controlled hybrid dynamics, we refer the readers to [7] and the references therein.

However, in systems with autonomous state jumps, these hybrid phenomena are tightly linked to the continuous control; thus, it is difficult to decouple the continuous control and the discrete phenomena. Compared with controlled hybrid systems, autonomous state jumps introduce extra nonlinearity into the problem due to the

*Princeton University

†Princeton University

‡Zhejiang University

§Peking University and Princeton University

¶Flatiron Institute (jiekunhan@gmail.com)

undetermined times and states at jumps. Furthermore, the total cost may change dramatically when the updated control triggers a new collision or avoids an existing collision in the solution process. These are all challenging issues for optimization.

Dynamic programming and trajectory optimization are two basic approaches for solving optimal control problems. Dynamic programming provides a global optimal closed-loop control based on Bellman’s principle of optimality [6]. It suffers from the curse of dimensionality and generally does not scale to high dimensional systems. Trajectory optimization solves for a locally optimal trajectory and usually provides an open-loop solution. Some methods lie in between, including differential dynamical programming (DDP) [26], iterative linear-quadratic regulator (iLQR) [30], sequential linear-quadratic control (SLQ) [45], and iterative linear-quadratic-Gaussian method (iLQG) [55]. These methods use linear or quadratic approximations around the nominal trajectory for the dynamics or costs to find a local closed-loop control. Since these methods require derivatives of the dynamics, some smoothing techniques that sacrifice accuracy are necessary for their applications in discontinuous systems [53, 34].

In this paper, we will tackle the discontinuous model directly and find the open-loop optimal control. There are two main categories of approaches for the open-loop optimal control problems: direct and indirect methods. Direct methods turn the infinite-dimensional control problems into finite-dimensional nonlinear programming problems through discretization; thus, they are often described as discretize-then-optimize. Being hybrid introduces extra difficulties. For example, the control problem of a frictional system is turned into a mixed-integer programming problem [18]. In [48], it is pointed out that the discretize-then-optimize approach may lead to incorrect gradients. In [5, 4], gradient-type algorithms are proposed for the autonomous hybrid systems where the adjoint equations are used to compute the gradients (with respect to the controls). In this approach, the discontinuity information is implicitly reflected in the gradients and thus influences the continuous controls when applying iterative gradient-based algorithms. Indirect methods use necessary conditions for the optimality of the control problem; they are often described as optimize-then-discretize. They turn the optimal control problem into a system of differential-algebraic equations. The necessary conditions are formulated for the continuous-time problem; thus, they have less to do with how the dynamical system is discretized. Pontryagin’s minimum principle (PMP) [40] is a well-known set of first-order necessary conditions in optimal control. Based on the hybrid maximum principle, an extension of PMP to the hybrid dynamical system, [43] proposed a numerical algorithm (HMP-MAS, short for hybrid maximum principle multiple autonomous switchings) that handles the discontinuities explicitly. For a (estimated) given number of switches and an initial guess of switching times and states, HMP-MAS alternates between computing the optimal controls inside each continuous interval and updating switching times and states by gradient descent. The constraints that switching states must be on the switching manifolds are enforced through the penalty method. This method was proposed for the switching system but can be extended to the state-jump system; see Section 5.4.

This paper proposes an iterative method for the open-loop optimal control of dynamical systems with autonomous state jumps (collisions). We begin with a hybrid minimum principle (HMP) which extends the PMP to the hybrid dynamical systems with autonomous state jumps. We then propose an algorithm based on the methods of successive approximation [15], with extra relaxation for convergence. The algorithm automatically avoids unnecessary collisions and does not require an accurate prediction of the number of collision times. It generally converges faster and produces

more accurate solutions than gradient-based algorithms. We implement the algorithm with the forward-Euler scheme and address several difficulties introduced by the discontinuities of the hybrid system. The method is tested on disc collision problems with one or multiple collisions. It exhibits stable linear convergence in terms of the iteration steps. Asymptotic first-order accuracy is observed for the L^2 error on model problems with exact analytic solutions.

This article is organized as follows. In Section 2, we formulate the dynamical systems. The hybrid minimum principle is presented in Section 3. An HMP-based numerical algorithm is introduced in Section 4, with several considerations on the numerical issues. We demonstrate the performance of the proposed algorithm for several examples in Section 5. Comparisons to the HMP-MAS, a direct method, and a deep reinforcement learning method are then discussed. Finally, we conclude in Section 6 with some discussions on possible extensions.

1.1. Notations. We will denote the state of the system by $\mathbf{x}(\cdot) \in \mathbb{R}^m$ and the control by $\mathbf{u}(\cdot) \in U \subset \mathbb{R}^{m_u}$. The time interval considered is always $[0, T]$. We use $|\mathbf{z}|$ to denote the Euclidean norm for any \mathbf{z} in the Euclidean space. For a scalar function $h = h(\mathbf{z}) : \mathbb{R}^n \rightarrow \mathbb{R}$, its derivative with respect to \mathbf{z} is a row vector $\partial_{\mathbf{z}} h = h_{\mathbf{z}} = [h_{z_1}, \dots, h_{z_n}]$. For a vector-valued function $\mathbf{h} = [h_1, \dots, h_k]^T : \mathbb{R}^n \rightarrow \mathbb{R}^k$, its Jacobian is defined as

$$\mathbf{h}_{\mathbf{z}} = \begin{bmatrix} \partial_{z_1} h_1 & \cdots & \partial_{z_n} h_1 \\ \partial_{z_1} h_2 & \cdots & \partial_{z_n} h_2 \\ \vdots & \ddots & \vdots \\ \partial_{z_1} h_k & \cdots & \partial_{z_n} h_k \end{bmatrix} \in \mathbb{R}^{k \times n}.$$

In two dimensions, we also use x, y as subscripts to denote the x, y coordinates, respectively.

2. Problem formulation. Given the initial condition $\mathbf{x}(0) = \mathbf{x}_0$ and the control process $\mathbf{u}(t)$, the evolution of state $\mathbf{x}(t)$ is governed by piecewise smooth dynamics:

$$\dot{\mathbf{x}}(t) = \mathbf{f}(\mathbf{x}(t), \mathbf{u}(t)), t \in (\gamma_i, \gamma_{i+1}), i = 0, \dots, K, \quad (2.1)$$

where $0 = \gamma_0 < \gamma_1 < \dots < \gamma_K < \gamma_{K+1} = T$. For each $i = 1, \dots, K$, a jump function g is applied on the state at time γ_i ,

$$\mathbf{x}(\gamma_i^+) = \mathbf{g}(\mathbf{x}(\gamma_i^-)). \quad (2.2)$$

Here $\mathbf{x}(\gamma_i^\pm)$ denote the value of \mathbf{x} at γ_i evaluated from the right/left time interval, *i.e.*, $\lim_{t \in (\gamma_i, \gamma_{i+1}), t \rightarrow \gamma_i} \mathbf{x}(t)$ / $\lim_{t \in (\gamma_{i-1}, \gamma_i), t \rightarrow \gamma_i} \mathbf{x}(t)$, respectively.

Note that the number of jumps K and the jump time γ_i are not prescribed; instead, they are functions of the control \mathbf{u} . They are determined by a ‘‘collision detection’’ function $\psi(\mathbf{x}) \geq 0$ that checks whether a jump of state occurs. Namely,

$$\psi(\mathbf{x}(\gamma_i^-)) = 0, \quad (2.3)$$

and $\psi(\mathbf{x}(\cdot)) > 0$ at γ_i^+ and all t other than γ_i^- . That is why we call such jumps as autonomous state jumps. We assume both ψ and \mathbf{g} are smooth in an open set containing $\{\mathbf{x} : \psi(\mathbf{x}) = 0\}$.

The optimal control problem is then formulated as

$$\begin{aligned} \underset{\mathbf{u}(\cdot)}{\text{minimize}} \quad & J(\mathbf{u}(\cdot)) = \phi(\mathbf{x}(T)) + \sum_{i=0}^K \int_{\gamma_i}^{\gamma_{i+1}} L(\mathbf{x}(t), \mathbf{u}(t)) dt, \quad (2.4a) \\ \text{subject to} \quad & \text{eqs. (2.1) to (2.3)}. \quad (2.4b) \end{aligned}$$

Here, ϕ is the terminal cost function, and L is the running cost function; both are smooth. We assume \mathbf{f}, ϕ, L to be all time-independent in this paper for the simplicity of notations. The minimum principle and numerical algorithm work for time-dependent \mathbf{f}, ϕ, L straightforwardly.

To ensure that the above model is well-posed, we shall require that the trajectory of the state \mathbf{x} transverses the manifold $\{\psi = 0\}$ where jumps of the state take place. That is, the state \mathbf{x} should not move tangentially on the manifold, or

$$0 \neq \frac{d}{dt}\psi(\mathbf{x}(t)) = \psi_x(\mathbf{x}(t))\dot{\mathbf{x}}(t) = [\psi_x \mathbf{f}]|_t. \quad (2.5)$$

Here ψ_x is the normal vector for the manifold and $\dot{\mathbf{x}} = \mathbf{f}$ is the instantaneous moving direction of the state \mathbf{x} . In the context of collisional rigid body dynamics, $\psi_x \mathbf{f}$ is the relative velocity projected to the contact normal vector, which should be nonzero for the collision to take place. See Section 5 for a concrete example.

3. Hybrid minimum principle. Pontryagin's maximum principle for standard optimal control can be extended to the discontinuous dynamics introduced here. We shall call this extension the hybrid minimum principle (HMP). To begin with, we introduce the *Hamiltonian* $H : \mathbb{R}^m \times \mathbb{R}^m \times U \rightarrow \mathbb{R}$

$$H(\mathbf{x}, \boldsymbol{\lambda}, \mathbf{u}) = \boldsymbol{\lambda}^T \mathbf{f}(\mathbf{x}, \mathbf{u}) + L(\mathbf{x}, \mathbf{u}). \quad (3.1)$$

THEOREM 3.1 (Hybrid Minimum Principle). *Let $\{\mathbf{x}(t), \mathbf{u}(t)\}$ be the optimal solution associated with (2.4), then there exists a costate process $\boldsymbol{\lambda}(t) : [0, T] \rightarrow \mathbb{R}^m$ that satisfies*

$$\dot{\boldsymbol{\lambda}}(t) = -H_x^T(\mathbf{x}(t), \boldsymbol{\lambda}(t), \mathbf{u}(t)), t \in (\gamma_i, \gamma_{i+1}), i = 0, \dots, K, \quad (3.2)$$

with the terminal condition

$$\boldsymbol{\lambda}(T) = \phi_x^T(\mathbf{x}(T)), \quad (3.3)$$

and backward jump conditions, $i = 1, \dots, K$,

$$\boldsymbol{\lambda}^T(\gamma_i^-) = \boldsymbol{\lambda}^T(\gamma_i^+) \mathbf{g}_x(\mathbf{x}(\gamma_i^-)) + \eta_i \psi_x(\mathbf{x}(\gamma_i^-)), \quad (3.4)$$

where $\eta_i \in \mathbb{R}$ satisfies the following equation (variation of collision time)

$$\boldsymbol{\lambda}^T(\gamma_i^+) \mathbf{g}_x(\mathbf{x}(\gamma_i^-)) \mathbf{f}|_{\gamma_i^-} - \boldsymbol{\lambda}^T(\gamma_i^+) \mathbf{f}|_{\gamma_i^+} + \eta_i \psi_x(\mathbf{x}(\gamma_i^-)) \mathbf{f}|_{\gamma_i^-} + L|_{\gamma_i^-} - L|_{\gamma_i^+} = 0. \quad (3.5)$$

Here, $h|_{s^\pm}$ denotes function h evaluated at s as limits from right and left, respectively. In addition, the optimal control \mathbf{u} minimizes the Hamiltonian for each $t \in [0, T]$:

$$\mathbf{u}(t) = \arg \min_{\mathbf{v} \in U} H(\mathbf{x}(t), \boldsymbol{\lambda}(t), \mathbf{v}). \quad (3.6)$$

We refer to [56] for a proof of this theorem. A few remarks on PMP and HMP are in order.

REMARK 1. *By the assumption of transversality eq. (2.5), we have $\psi_x \mathbf{f} \neq 0$ when $\psi = 0$. Therefore the equation eq. (3.5) is always non-degenerate. We note that the condition eq. (3.5) from variation of collision time is equivalent to the Hamiltonian constancy condition quoted in other literature, i.e. $H|_{\gamma_i^-} = H|_{\gamma_i^+}$.*

REMARK 2. *We have omitted the abnormal multiplier in the statement of Theorem 3.1 for brevity. In a more complete form, there is a technicality involving multiplier $\lambda_0 \geq 0$ in the Hamiltonian (3.1) $H = \boldsymbol{\lambda}^T \mathbf{f} + \lambda_0 L$ and in the terminal condition (3.3) $\boldsymbol{\lambda}(T) = \lambda_0 \phi_x^T(\mathbf{x}(T))$. Besides, the λ_0 also presents in front of $L|_{\gamma_i^-}, L|_{\gamma_i^+}$ in eq. (3.5), which can be seen from its equivalence to $H|_{\gamma_i^-} = H|_{\gamma_i^+}$. In the case where $\lambda_0 = 0$ is the only candidate, the problem is singular and, in some sense, ill-posed [2]. Otherwise, we can rescale the costate $\boldsymbol{\lambda}$ so that we can always let $\lambda_0 = 1$ (note that the additional η_i in eqs. (3.4) and (3.5) does not prevent $\boldsymbol{\lambda}$ from rescaling). We shall only consider this case and take $\lambda_0 = 1$ in this paper.*

REMARK 3. *Most proofs of PMP and HMP resort to the calculus of variations with some special classes of control variations. We note that, H_u can be interpreted as the Fréchet derivative of the reduced total cost \hat{J} with respect to control function \mathbf{u} in L^2 , where*

$$\hat{J}(\mathbf{u}(\cdot)) = \phi(\mathbf{x}(T; \mathbf{u}(\cdot))) + \sum_{i=0}^K \int_{\gamma_i}^{\gamma_{i+1}} L(\mathbf{x}(t; \mathbf{u}(\cdot)), \mathbf{u}(t)) dt,$$

and $\mathbf{x}(t; \mathbf{u}(\cdot))$ denotes the trajectory obtained with control $\mathbf{u}(\cdot)$ according to eqs. (2.1) to (2.3). This argument and its proof is often a step in the complete proof of the PMP and HMP. For a formal derivation, see Chapter 6.2 of [54]. For a rigorous proof, see the proof of necessary conditions of optimality in Chapter 1.4 [25] on continuous dynamics and see those proof of the HMP (e.g. [56]) for the present case.

REMARK 4. *The PMP/HMP is related to the Karush-Kuhn-Tucker (KKT) conditions for constrained optimization problems. In fact, the dynamic equations of \mathbf{x} (eqs. (2.1) to (2.3)) can be viewed as an infinite-dimensional constraint. The costate $\boldsymbol{\lambda}$ plays the role of a continuous-time analogy of the Lagrange multiplier. The HMP/PMP is stronger than the KKT conditions in the sense that it asserts that H is not only stationary but also minimized at the optimal control (eq. (3.6)). Like KKT, the PMP/HMP is only a set of necessary conditions. However, these sets of necessary conditions are often sufficient to provide a good (even optimal) solution given a reasonable initial guess.*

REMARK 5. *HMP has been studied extensively in the literature. In [49, 21], HMP has been formulated and proved for a general framework of the hybrid dynamic systems. The HMP is proved by reducing the optimal control problem of the hybrid system to the canonical Pontryagin type in [17]. Adding pathwise inequality constraints to the control problem will append related complementary equations to the resulting HMP [13]. In [3], the HMP has been derived for autonomous hybrid dynamical systems whose jump magnitudes are additional control variables. The HMP has also been extended to manifolds where the costate is a trajectory on the cotangent bundle [52].*

4. Algorithm. In this section, we develop an algorithm based on the HMP in Theorem 3.1 to solve the optimal control problem with hybrid dynamics. At a high level, given a control, the forward equations (2.1) to (2.3) for the state $\mathbf{x}(\cdot)$ and the

backward equations (3.2) to (3.5) for the costate $\boldsymbol{\lambda}(\cdot)$ are satisfied by solving the corresponding forward and backward problems, respectively. It remains to find the optimal control $\mathbf{u}(\cdot)$ such that (3.6) is also satisfied. To this end, we propose an iterative method. In the k -th iteration, given the control $\mathbf{u}^k(\cdot)$, we compute $\mathbf{x}^k(\cdot), \boldsymbol{\lambda}^k(\cdot)$ by solving the forward and backward dynamics, respectively. We then update the control using the information from minimizing the Hamiltonian (3.6). To be specific, we define the minimizer $\mathbf{u}_*^{k+1}(\cdot)$ in the k -th iteration by

$$\mathbf{u}_*^{k+1}(t) = \arg \min_{\mathbf{v} \in U} H(\mathbf{x}^k(t), \boldsymbol{\lambda}^k(t), \mathbf{v}), \quad \forall t \in [0, T]. \quad (4.1)$$

The control is then updated by

$$\mathbf{u}^{k+1}(t) = (1 - \alpha)\mathbf{u}^k(t) + \alpha\mathbf{u}_*^{k+1}(t), \quad \forall t \in [0, T]. \quad (4.2)$$

where $\alpha > 0$ is a small relaxation parameter.

We remark that when $\alpha = 1$ in eq. (4.2), the algorithm above is called the method of successive approximations [15]. This method converges for a restricted class of linear systems [1] but may diverge in general. The reason is that the control \mathbf{u}_*^{k+1} based on the trajectories $\mathbf{x}^k, \boldsymbol{\lambda}^k$ simulated with the control \mathbf{u}^k may not be close enough to \mathbf{u}^k , so the corresponding trajectories may not be close enough, and the total objective may even increase if the change is too much (see [29] for a more detailed explanation). In [29], an extended version of the method of successive approximations is proposed to penalize the deviations from the dynamic constraints on the state and costate, *i.e.*, $\dot{\mathbf{x}}^k - H_{\mathbf{x}}(\mathbf{x}^k, \boldsymbol{\lambda}^k, \mathbf{u}^{k+1})$ and $\dot{\boldsymbol{\lambda}}^k + H_{\mathbf{x}}(\mathbf{x}^k, \boldsymbol{\lambda}^k, \mathbf{u}^{k+1})$. Here we choose to use a small α in eq. (4.2) to restrict the update of the control from the minimization step of the Hamiltonian so that the state and costate will not change too much in the next iteration.

We now discuss the numerical implementation of the iterative scheme presented above. Each iteration consists of the following four steps.

1. Using control from the last iteration, we numerically simulate the forward dynamics eqs. (2.1) to (2.3) using the forward-Euler scheme with the collision times prediction. The active collision indexes and the states before and after collisions are gathered for the backward dynamics in the simulation.
2. Solve the backward dynamics eqs. (3.2) to (3.5) using the forward Euler scheme (backward in time) and the gathered collision information.
3. Update the control pointwise in time according to eqs. (4.1) and (4.2) with the newly computed state and costate.
4. Check whether convergence has been achieved.

The whole algorithm is summarized in Algorithm 1. It remains to solve each subprogram in Algorithm 1 with proper time discretization. To this end, we discretize the time interval $[0, T]$ into N uniform intervals: $t_n = n\Delta t$, $n = 0, \dots, N$, $\Delta t = \frac{T}{N}$. When describing the discretization of the forward and backward dynamics below, we drop the iteration superscript k for simplicity. $\mathbf{x}_n, \boldsymbol{\lambda}_n, \mathbf{u}_n$ denote the numerical approximations of the state, costate and control at t_n , respectively. Now we describe each subprogram in detail.

Forward dynamics. The numerical simulation of a hybrid dynamical system with discontinuities is not a simple task, and there are many related works in the literature [14, 20, 44, 11, 12]. The key idea involves an accurate estimation of the collision time using a root-finding scheme and a proper integration step around the collision by a variable-step integrator. Our integrator estimates the collision time based on a

linear approximation and adds an intermediate time step at the estimated time. To be specific, at each step, we estimate the collision time by solving the equation

$$s_n = s(\mathbf{x}_n, \mathbf{u}_n) = \inf\{s > 0 : \psi(\mathbf{x}_n + s\mathbf{f}(\mathbf{x}_n, \mathbf{u}_n)) = 0\}. \quad (4.3)$$

Here, $s_n = \infty$ means the set of solutions is empty, *i.e.* no collision predicted from the current state x_n with control u_n . If $s_n < \Delta t$, we then insert an extra integration step at $t_n + s_n$ and apply the jump function g at this step. The forward dynamics is summarized as follows,

$$\left\{ \begin{array}{l} \text{If } s_n = s(\mathbf{x}_n, \mathbf{u}_n) < \Delta t, \\ \text{If } s_n = s(\mathbf{x}_n, \mathbf{u}_n) \geq \Delta t, \end{array} \right. \left\{ \begin{array}{l} \mathbf{x}_{n+\frac{1}{2}}^- = \mathbf{x}_n + s_n \mathbf{f}(\mathbf{x}_n, \mathbf{u}_n), \\ \mathbf{x}_{n+\frac{1}{2}}^+ = \mathbf{g}(\mathbf{x}_{n+\frac{1}{2}}^-), \\ \mathbf{x}_{n+1} = \mathbf{x}_{n+\frac{1}{2}}^+ + (\Delta t - s_n) \mathbf{f}(\mathbf{x}_{n+\frac{1}{2}}^+, \mathbf{u}_{n+\frac{1}{2}}^+), \\ \mathbf{x}_{n+1} = \mathbf{x}_n + \Delta t \mathbf{f}(\mathbf{x}_n, \mathbf{u}_n), \end{array} \right. \quad (4.4)$$

for $n = 0, \dots, N-1$. Here $\mathbf{u}_{n+\frac{1}{2}}^+ = \mathbf{u}_{n+1}$ if we only have discrete sequence of the control at t_n . We note that the estimation of the collision time does not add much complexity to the simulation in practice. At most integration steps t_n where no collision happens within a time step, a fast but rough estimation of s_n is sufficient. This paper focuses on controlling such dynamical systems. The readers interested in convergence may consult [36, 37] for a rigorous analysis of similar dynamics.

After the forward simulation according to (4.4), we define the active collision index set \mathcal{C} to include those n such that $s_n < \Delta t$ in simulation,

$$\mathcal{C} = \{n : s_n < \Delta t\}. \quad (4.5)$$

Backward dynamics. The discretization of the backward costate equations (3.2) to (3.5) is similar. With the terminal condition $\lambda_N = \phi_x^T(\mathbf{x}_N, t_N)$, for $n = N-1, N-2, \dots, 1$, we have

$$\lambda_n = \lambda_{n+1} + \Delta t H_x^T(\mathbf{x}_n, \lambda_{n+1}, \mathbf{u}_n), \quad \text{if } n \notin \mathcal{C}, \quad (4.6)$$

and if $n \in \mathcal{C}$,

$$\lambda_{n+\frac{1}{2}}^+ = \lambda_{n+1} + (\Delta t - s_n) H_x^T(\mathbf{x}_{n+\frac{1}{2}}^+, \lambda_{n+1}, \mathbf{u}_{n+\frac{1}{2}}^+), \quad (4.7a)$$

$$\lambda_{n+\frac{1}{2}}^- = \mathbf{G}(\lambda_{n+\frac{1}{2}}^+, \mathbf{x}_{n+\frac{1}{2}}^-, \eta(\lambda_{n+\frac{1}{2}}^+, \mathbf{x}_{n+\frac{1}{2}}^+, \mathbf{x}_{n+\frac{1}{2}}^-, \mathbf{u}_{n+\frac{1}{2}}^+, \mathbf{u}_{n+\frac{1}{2}}^-)), \quad (4.7b)$$

$$\lambda_n = \lambda_{n+\frac{1}{2}}^- + s_n H_x^T(\mathbf{x}_n, \lambda_{n+\frac{1}{2}}^-, \mathbf{u}_n). \quad (4.7c)$$

Here we combine eqs. (3.4) and (3.5) into the function \mathbf{G} for simplicity, where $\lambda(t_i^-) = \mathbf{G}(\lambda(t_i^+), \mathbf{x}(t_i^-), \eta)$ is defined by (3.4), and $\eta = \eta(\lambda(t_i^+), \mathbf{x}(t_i^+), \mathbf{x}(t_i^-), \mathbf{u}(t_i^+), \mathbf{u}(t_i^-))$ is defined by (3.5).

In practice, the discontinuities will introduce numerical instability, especially when solving eq. (4.7b). The factor Δt is missing in eq. (4.7b), whose detailed definition comes from eqs. (3.4) and (3.5). This fact implies that, for $c \in \mathcal{C}$, an $O(1)$ error in $\mathbf{u}_{c+\frac{1}{2}}^\pm$ will bring up an $O(1)$ error in λ_c from eq. (4.7b), and thus $O(1)$ errors in all $\lambda_k, k \leq c$. This is distinct from eqs. (4.4) and (4.6) when the dynamics is continuous and there is always a factor Δt . Therefore, some extra numerical treatments are needed in order to ensure numerical stability and convergence speed when estimating $\mathbf{u}_{c+\frac{1}{2}}^+, \mathbf{u}_{c+\frac{1}{2}}^-$ in evaluating (4.7). Physically, these two values represent the values of

the control after and before the collision, respectively. The following two paragraphs are devoted to a better estimation of $\mathbf{u}_{c+\frac{1}{2}}^+, \mathbf{u}_{c+\frac{1}{2}}^-$.

Ideally, the discontinuities of the optimal control and collisions should occur simultaneously. However, in the algorithm with time discretization, they can misalign before convergence due to the relaxed updating rule of \mathbf{u} in eq. (4.2). During iterations, we observe significant delays in the discontinuities of the control in response to the shifting discontinuities in the state \mathbf{x} . For each $c \in \mathcal{C}$, an inappropriate estimation of $\mathbf{u}_{c+\frac{1}{2}}^+, \mathbf{u}_{c+\frac{1}{2}}^-$ will slowdown the convergence and even worse prevent the algorithm from converging. Instead of using the control values $\mathbf{u}_{c+1}, \mathbf{u}_c$ closest to the collision, we propose to use the steepest varying control values near the collision. To be specific, we find

$$c^* = \arg \max_{|n-c|<l} |\mathbf{u}_n - \mathbf{u}_{n+1}|, \quad (4.8)$$

where l is a given integer. Then the information around t_{c^*} will be used to determine $\mathbf{u}_{c+\frac{1}{2}}^+, \mathbf{u}_{c+\frac{1}{2}}^-$, as explained in the next paragraph. In practice, we choose $l = \tau N, \tau \in (0, 1)$ so that the range in which we search for the discontinuity is independent of the discretization. Namely, we resolve better control estimations locally in $(t_c - \tau T, t_c + \tau T)$, where $t_c = c\Delta t$. τT should be less than the shortest time between adjacent collisions. In our experiments presented in Section 5, we always take $\tau = 0.05$.

In the experiments, we also observe that the convergence of the control around collisions is much slower (or even not convergent). This phenomenon is caused by the discontinuities in the control and the fluctuation of simulated collision indexes. To be specific, let us focus on a collision index $c \in \mathcal{C}$. From the forward dynamics eq. (4.4) and the backward dynamics eq. (4.7), the state \mathbf{x} and costate $\boldsymbol{\lambda}$ change discontinuously from c to $c+1$ and from $c+1$ to c , respectively. Then, the control values $\mathbf{u}_c, \mathbf{u}_{c+1}$ are updated to different values when applying eqs. (4.10) and (4.11). If in the next iteration, this collision index shifts from c , for example, to $c' = c+1$, $\mathbf{u}_{c'} = \mathbf{u}_{c+1}$ will update to the “before-collision” target. Then, \mathbf{u}_{c+1} would oscillate between two different values without convergence. In other words, the control values around collisions might approach two distinct targets $\mathbf{u}^{opt,-}, \mathbf{u}^{opt,+}$ alternatively and thus oscillate between these two targets endlessly, where $\mathbf{u}^{opt,-}, \mathbf{u}^{opt,+}$ are the optimal controls before/after a collision, respectively. To avoid this oscillation, we should rely on the control values farther from the collisions to make more stable estimations since the controls are continuous in each segment. As the control after/before a collision is right/left continuous, we will use the control values after/before the collision to approximate $\mathbf{u}_{c+\frac{1}{2}}^+/\mathbf{u}_{c+\frac{1}{2}}^-$. To be specific, when estimating $\mathbf{u}_{c+\frac{1}{2}}^+, \mathbf{u}_{c+\frac{1}{2}}^-$, instead of using the control values at c^*+1, c^* from eq. (4.8), we extrapolate them by the control values in $\mathcal{I}_{j,p}^+ = \{c^*+1+i : i \in \{j, \dots, p\}\}$ and $\mathcal{I}_{j,p}^- = \{c^*-i : i \in \{j, \dots, p\}\}$, respectively, where $p \geq j \geq 1$ are integers. In this paper, we choose the simple approach corresponding to $j = p = 1$:

$$\mathbf{u}_{c+\frac{1}{2}}^+ = \mathbf{u}_{c^*+2}, \quad \mathbf{u}_{c+\frac{1}{2}}^- = \mathbf{u}_{c^*-1}. \quad (4.9)$$

We remark that choosing p and the extrapolation scheme depends on the desired order of accuracy and the stability of underlying dynamics, which reflects a trade-off between stability and accuracy. If a higher-order integration scheme is applied to solve the forward and backward dynamics, one should apply a higher-order extrapolation method with $p > j$. Besides, one may take larger p, j if the unstable dynamics brings

large fluctuations in the collision times during iterations. We note that other than the accuracy concerns, the distances (in time t) to adjacent collisions prohibit selecting large p .

Updating the control. It remains to discretize the equation (4.1). From the discretization of $\mathbf{x}, \boldsymbol{\lambda}$ described above, we have $\mathbf{x}_0^k, \dots, \mathbf{x}_N^k$ and $\boldsymbol{\lambda}_1^k, \dots, \boldsymbol{\lambda}_N^k$ in the k -th step by using \mathbf{u}^k , and we need to update the control at t_0, \dots, t_{N-1} . Note that the control at $t_N = T$ is not used in the discretized forward and backward dynamics; thus, we do not need to update it. For each \mathbf{u}_n to be updated, the costate information should be backpropagated from $\boldsymbol{\lambda}_{n+1}$. So we apply the following rule at each time step n ,

$$\mathbf{u}_{*,n}^{k+1} = \arg \min_{\mathbf{v} \in U} H(\mathbf{x}_n^k, \boldsymbol{\lambda}_{n+1}^k, \mathbf{v}), \quad n = 0, \dots, N-1. \quad (4.10)$$

We then discretize eq. (4.2) straightforwardly in a pointwise manner:

$$\mathbf{u}_n^{k+1} = (1 - \alpha)\mathbf{u}_n^k + \alpha\mathbf{u}_{*,n}^{k+1}, \quad n = 0, \dots, N-1. \quad (4.11)$$

Equation (4.10) defines a finite-dimensional optimization problem for each n , which can be solved in parallel. In cases like the examples considered in this paper, there are analytical expressions for the minimizers of the Hamiltonian. If H is convex in \mathbf{u} for fixed $\mathbf{x}, \boldsymbol{\lambda}$, many efficient convex optimization algorithms can be used. Otherwise, a general numerical optimizer can also perform well with the initial guesses from the last iterations and adjacent grids.

We should mention that the above choice of indexes for \mathbf{x} and $\boldsymbol{\lambda}$ at time step n is also consistent with the discretize-then-optimize approach. Namely, consider the following discrete problem without any collision

$$\underset{\mathbf{u}_0, \dots, \mathbf{u}_{N-1}}{\text{minimize}} \quad \phi(\mathbf{x}_N) + \sum_{i=0}^{N-1} L(\mathbf{x}_i, \mathbf{u}_i)\Delta t, \quad (4.12a)$$

$$\text{subject to} \quad \mathbf{x}_{n+1} = \mathbf{x}_n + \Delta t \mathbf{f}(\mathbf{x}_n, \mathbf{u}_n). \quad (4.12b)$$

If we introduce the Lagrange multiplier $\boldsymbol{\lambda}_n$ corresponding to the dynamic constraint at each time step and derive the first-order necessary condition, we will have

$$H_u(\mathbf{x}_{*,n}, \boldsymbol{\lambda}_{*,n+1}, \mathbf{u}_{*,n}) = 0, \quad (4.13)$$

where the subscript $*$ denotes the optimal solution for the discrete problem. We can see that the time indexes in eq. (4.13) are consistent with those in eq. (4.10).

Convergence test. Since the forward dynamics of \mathbf{x} and the backward dynamics of $\boldsymbol{\lambda}$ are always solved accurately in the previous steps, we only need to check the Hamiltonian minimization condition eq. (3.6) to decide whether convergence is achieved. The L^2 norm of H_u (eq. (3.6)) serves as a natural convergence indicator. As pointed out in Remark 3, H_u also has the meaning of the derivative of the total cost with the control \mathbf{u} . Given $\mathbf{u}^k = [\mathbf{u}_0^k, \dots, \mathbf{u}_{N-1}^k]$, H_u is discretized as

$$H_{u,n}^k = H_u(\mathbf{x}_n^k, \boldsymbol{\lambda}_{n+1}^k, \mathbf{u}_n^k), \quad n = 0, \dots, N-1. \quad (4.14)$$

The indexes relation follows the same logic as in eq. (4.10). We then compute the numerical L^2 norm as

$$\sqrt{\sum_{n=0}^{N-1} (H_{u,n}^k)^2 \Delta t}. \quad (4.15)$$

We stop the algorithm when the above quantity is less than a pre-specified tolerance number δ .

Algorithm 1 HMP based algorithm for optimal control with hybrid dynamics

input the number of discretization time intervals N , the initial guess of the control $\mathbf{u}^0 = [\mathbf{u}_0^0, \mathbf{u}_1^0, \dots, \mathbf{u}_{N-1}^0]$, the convergence criteria $\delta > 0$.

$k \leftarrow 0$

while True **do**

Program Forward

 Apply eqs. (4.3) and (4.4) to get $\mathbf{x}^k = [\mathbf{x}_0^k, \mathbf{x}_1^k, \dots, \mathbf{x}_N^k]$, the active collision indexes set \mathcal{C} defined in eq. (4.5), and the states $\mathbf{x}_{c+\frac{1}{2}}^\pm$ around collision for $c \in \mathcal{C}$.

Program Backward

 Using computed \mathbf{x}^k and derived information around collisions, obtain $\boldsymbol{\lambda}^k = [\boldsymbol{\lambda}_1^k, \dots, \boldsymbol{\lambda}_N^k]$ by solving the backward dynamics with jumps described in eqs. (4.6) and (4.7). The control values $\mathbf{u}_{c+\frac{1}{2}}^\pm$ in eq. (4.7) are computed by combining eqs. (4.8) and (4.9).

Program Control Update

 Get control $\mathbf{u}^{k+1} = [\mathbf{u}_0^{k+1}, \dots, \mathbf{u}_{N-1}^{k+1}]$ according to eqs. (4.10) and (4.11).

Program Convergence Test

 Compute discrete L^2 norm of H_u according to eq. (4.15). If it is less than δ , return the controls \mathbf{u}^k .

$k \leftarrow k + 1$

end while

return the optimal control \mathbf{u}^k

5. Experiments. This paper mainly focuses on those hybrid dynamics whose difficulties are introduced by collisions. We will demonstrate the performance of the Algorithm 1 in this scenario by applying it to the rigid body dynamics for a system composed of two-dimensional discs without frictional forces. These discs are homogeneous and fully characterized by their masses and radii. We remove the degrees of freedom associated with the orientations and angular velocities as these quantities are constant in the frictionless rigid body dynamics of discs.

There are always two discs in the following experiments. Denote the masses of these two discs by m_1, m_2 and the radii by r_1, r_2 . In this paper, we always take $m_1 = m_2 = 1, r_1 = r_2 = 0.2$ and the coefficient of restitution $C_R = 1$, *i.e.* perfectly elastic collision. These parameters are summarized in Table 5.1. We control disc 1 by

TABLE 5.1
Common parameters for all experiments

mass		radius		coefficient of restitution
m_1	m_2	r_1	r_2	C_R
1	1	0.2	0.2	1

applying a force to it so that it collides with disc 2 in a way that disc 2 will be close

to the prescribed locations at the terminal time T . Due to the translation invariance, the terminal location is always set to the origin $(0, 0)$. The running cost is the L^2 norm of the applied force.

Below we specify the control problem in terms of the equations eqs. (2.1) to (2.4). The state \mathbf{x} is composed of the positions and velocities of the two discs, *i.e.* $\mathbf{x} \in \mathbb{R}^8$. Let us write $\mathbf{x} = [\mathbf{x}_{q_1}^T, \mathbf{x}_{q_2}^T, \mathbf{x}_{v_1}^T, \mathbf{x}_{v_2}^T]^T$, where $\mathbf{x}_{q_i}, \mathbf{x}_{v_i}$ are the position and the velocity of disc i , respectively. We similarly write $\boldsymbol{\lambda} = [\boldsymbol{\lambda}_{q_1}^T, \boldsymbol{\lambda}_{q_2}^T, \boldsymbol{\lambda}_{v_1}^T, \boldsymbol{\lambda}_{v_2}^T]^T$.

The dynamics of two discs. The control $\mathbf{u} \in \mathbb{R}^2$ denotes the force applied to disc 1. The field \mathbf{f} is

$$\mathbf{f}(\mathbf{x}, \mathbf{u}) = \begin{pmatrix} 0_4 & I_4 \\ 0_4 & 0_4 \end{pmatrix} \mathbf{x} + \begin{pmatrix} 0_{4 \times 2} \\ M_1^{-1} \\ 0_{2 \times 2} \end{pmatrix} \mathbf{u}, \quad (5.1)$$

where I_4 is a 4×4 identity matrix and $M_1 = \text{diag}(m_1, m_1)$ is the inertial matrix. $0_k = 0_{k \times k}, 0_{m \times n}$ are zero matrices.

The collision function. The contact normal vector \mathbf{n} is the unit vector in the collision axis

$$\mathbf{n} = \frac{\mathbf{x}_{q_1} - \mathbf{x}_{q_2}}{|\mathbf{x}_{q_1} - \mathbf{x}_{q_2}|}. \quad (5.2)$$

We denote $\mathbf{v}_1 = \mathbf{x}_{v_1}, \mathbf{v}_2 = \mathbf{x}_{v_2}$ for simplicity. Let $\mathbf{v}_{i,E}, i = 1, 2$ be the velocities after (elastic) collision,

$$\begin{aligned} \mathbf{v}_{1,E} &= \mathbf{v}_1 - \frac{2m_2(\mathbf{v}_1 - \mathbf{v}_2) \cdot \mathbf{n}}{m_1 + m_2} \mathbf{n}, \\ \mathbf{v}_{2,E} &= \mathbf{v}_2 + \frac{2m_1(\mathbf{v}_1 - \mathbf{v}_2) \cdot \mathbf{n}}{m_1 + m_2} \mathbf{n}. \end{aligned}$$

Then the after collision velocities are,

$$\mathbf{v}_{1,*} = \mathbf{v}_{1,E} + (C_R - 1)(\mathbf{v}_{1,E} \cdot \mathbf{n})\mathbf{n} - (C_R - 1)(\mathbf{v}_{\text{COM}} \cdot \mathbf{n})\mathbf{n}, \quad (5.4a)$$

$$\mathbf{v}_{2,*} = \mathbf{v}_{2,E} + (C_R - 1)(\mathbf{v}_{2,E} \cdot \mathbf{n})\mathbf{n} - (C_R - 1)(\mathbf{v}_{\text{COM}} \cdot \mathbf{n})\mathbf{n}, \quad (5.4b)$$

where $C_R \in [0, 1]$ is the coefficient of restitution and $\mathbf{v}_{\text{COM}} = (m_1\mathbf{v}_1 + m_2\mathbf{v}_2)/(m_1 + m_2)$ is the center of mass velocity for the two disc system. The positional components of \mathbf{g} are kept unchanged. In summary, the collision function \mathbf{g} is,

$$\mathbf{g}(\mathbf{x}) = [\mathbf{x}_{q_1}^T, \mathbf{x}_{q_2}^T, \mathbf{v}_{1,*}^T, \mathbf{v}_{2,*}^T]^T. \quad (5.5)$$

The collision detection. In the problems considered here, collisions happen when the distance between the two bodies equals to 0, and tends to decrease further. The distance between the two discs can be computed by subtracting the sum of their radii from the distance between their centers. The distance will keep decreasing if $(\mathbf{x}_{q_1} - \mathbf{x}_{q_2}) \cdot (\mathbf{x}_{v_1} - \mathbf{x}_{v_2}) < 0$, or equivalently, $\mathbf{n} \cdot (\mathbf{x}_{v_1} - \mathbf{x}_{v_2}) < 0$, recalling that \mathbf{n} is the contact normal defined in eq. (5.2). Therefore, we can take

$$\psi(\mathbf{x}) = \begin{cases} \|\mathbf{x}_{q_1} - \mathbf{x}_{q_2}\| - r_1 - r_2 & \text{if } \mathbf{n} \cdot (\mathbf{x}_{v_1} - \mathbf{x}_{v_2}) < 0 \\ 1 & \text{elsewhere} \end{cases}, \quad (5.6)$$

Note that though ψ is not continuous in \mathbb{R}^8 , it is smooth in the following open set of interest with some $0 < \beta < r_1 + r_2$

$$\{\mathbf{x} \in \mathbb{R}^8 : (\mathbf{x}_{q_1} - \mathbf{x}_{q_2}) \cdot (\mathbf{x}_{v_1} - \mathbf{x}_{v_2}) < 0, |\mathbf{x}_{q_1} - \mathbf{x}_{q_2}| > \beta\}.$$

For \mathbf{x} in this set,

$$\psi_x(\mathbf{x}) = [\mathbf{n}, -\mathbf{n}, 0_2, 0_2],$$

where $0_2 \in \mathbb{R}^2$ is the zero vector. We note that the dot product $\psi_x \mathbf{f} = \mathbf{n} \cdot (\mathbf{x}_{v_1} - \mathbf{x}_{v_2})$ is the relative velocity, whose negativity implies that η can be solved from eq. (3.5).

The control objective. The terminal cost term ϕ is taken to be the distance between disc 2 and the origin,

$$\phi(\mathbf{x}) = |\mathbf{x}_{q_2}|^2. \quad (5.7)$$

The running cost L is

$$L(\mathbf{x}, \mathbf{u}) = \epsilon |\mathbf{u}|^2, \quad (5.8)$$

where $\epsilon > 0$ is a fixed parameter.

The Hamiltonian. The Hamiltonian for the problem is given by,

$$H(\mathbf{x}, \boldsymbol{\lambda}, \mathbf{u}) = \boldsymbol{\lambda}_{q_1} \cdot \mathbf{x}_{v_1} + \boldsymbol{\lambda}_{q_2} \cdot \mathbf{x}_{v_2} + \boldsymbol{\lambda}_{v_1} \cdot \mathbf{u} + \epsilon |\mathbf{u}|^2. \quad (5.9)$$

Thus, the direct minimizer of H is,

$$\mathbf{u}_* = \arg \min_{\mathbf{v}} H(\mathbf{x}, \boldsymbol{\lambda}, \mathbf{v}) = -\frac{\boldsymbol{\lambda}_{v_1}}{2\epsilon}, \quad (5.10)$$

and H_u is

$$H_u(\mathbf{x}, \boldsymbol{\lambda}, \mathbf{u}) = \boldsymbol{\lambda}_{v_1} + 2\epsilon \mathbf{u}. \quad (5.11)$$

Like most iterative algorithms in nonlinear optimal control, a suitable initial guess is necessary for avoiding undesired local minima. This is more demanding for the discontinuous systems considered in this paper. For instance, in our disc collision problems, the terminal cost only depends on disc 2, and the control only accelerates disc 1. If the initial control does not trigger a state jump of disc 2, any local optimization algorithm is likely to converge to zero control ($\mathbf{u} = 0$) since the derivative of the total cost with respect to the control u vanishes at zero control (see Remark 3). To avoid this and facilitate the convergence to the global minimum, we choose the initial controls so that all the desired collision pairs (disc 1 and disc 2, disc 2 and wall) will be encountered. Details are provided in each subsection below.

To describe and quantify the performance of the algorithm, we define the L^2 semi-norm of a square integrable function $l(\cdot) : [0, T] \rightarrow \mathbb{R}$ as,

$$\|l\|_2 = \left[\frac{1}{T - 2\omega} \left(\int_0^{t_c - \omega} l^2(t) dt + \int_{t_c + \omega}^T l^2(t) dt \right) \right]^{1/2}, \quad (5.12)$$

when there is only one collision in the optimal trajectory and t_c denotes the corresponding collision time. In the integral, we are excluding a small interval with length

$2\omega > 0$ around the collision time. When there are multiple collisions, the semi-norm can be defined similarly. For a vector-valued function $\mathbf{h} = [h_x, h_y]^T$, we define its L^2 semi-norm as

$$\|\mathbf{h}\|_2 = (\|h_x\|_2^2 + \|h_y\|_2^2)^{1/2}. \quad (5.13)$$

Note that we always use x, y subscripts to denote the x, y coordinates since our experiments are in 2D. This semi-norm can better measure the distance between the simulated numerical control and the analytical one than the L^2 norm. The reason is that a tiny shift of the collision time may introduce a relatively large numerical difference in the controls (and the L^2 norm), which nevertheless has negligible effects on the dynamics. One should take ω to be larger than the smallest discretization size Δt . In the experiments, we take $\omega = 0.05T$.

In the following experiments, we will always denote the analytical solution for the optimal control by \mathbf{u}^{opt} , the total objective by J , and the optimal values of the objective by J^{opt} . We will denote the simulated optimal first collision time by s and its analytical solution by s^{opt} .

5.1. Concentric collision. We first consider the case when the optimal control is to drive disc 1 to hit disc 2 concentrically. We take the initial state as $\mathbf{q}_1 = [-2, -2]^T, \mathbf{q}_2 = [-1, -1]^T, \mathbf{v}_1 = \mathbf{v}_2 = [0, 0]^T$ and $\epsilon = 0.1, T = 1$. The objective is to push disc 1 to strike disc 2 so that disc 2 will be close to the origin at the terminal time $T = 1$. See Figure 5.1a for an illustration of the setup.

We discretize the dynamics into 480 steps, *i.e.* $N = 480$ and run the Algorithm 1 with the relaxation parameter $\alpha = 0.01$. The initial control can be any force fields that make collisions between the two discs happen. Here we take a constant force $[3, 3]^T$. The optimal analytical control for this example can be solved to machine accuracy; see Appendix A. See also Figure 5.1a for the optimal trajectories under the optimal control. We have shown and compared the simulated numerical control and the analytical optimal control, see Figure 5.1b.

In Figure 5.2, we visualize the solution process by showing how the cost, $\|H_u\|_2$, and $\|\mathbf{u} - \mathbf{u}^{opt}\|_2$ converge during the iteration. We can see that the algorithm converges well in a few hundred iterations. Besides, the convergence indicator $\|H_u\|_2$ indicates that the algorithm converges linearly for this example.

We repeated the experiments for $N = 60, 120, \dots, 1200$. We find that the numerical solution for the optimal control converges to the analytical solution and that the simulated collision times also converge to the analytical solution. Perfect first-order accuracy is observed; see Figure 5.3.

5.2. General situation for two discs. This experiment shows that our algorithm performs well in more general situations, *i.e.* relative velocity forms a non-zero angle with the axis of collision. We take the initial state to be $\mathbf{q}_1 = [-1, -2]^T, \mathbf{q}_2 = [-1, -1]^T, \mathbf{v}_1 = \mathbf{v}_2 = [0, 0]^T$ and $\epsilon = 0.01, T = 1$. See Figure 5.4a for an illustration of the setup.

We discretize the dynamics into 480 steps, *i.e.* $N = 480$ and run the Algorithm 1 with the relaxation parameter $\alpha = 0.01$. The initial control is a constant field $[0, 3]^T$ under which disc 1 collides with disc 2. The analytical solution can also be found for this problem, see Appendix A for the derivation and Figure 5.4a for the optimal trajectories. The numerical result is shown and compared to the analytical one in Figure 5.4b.

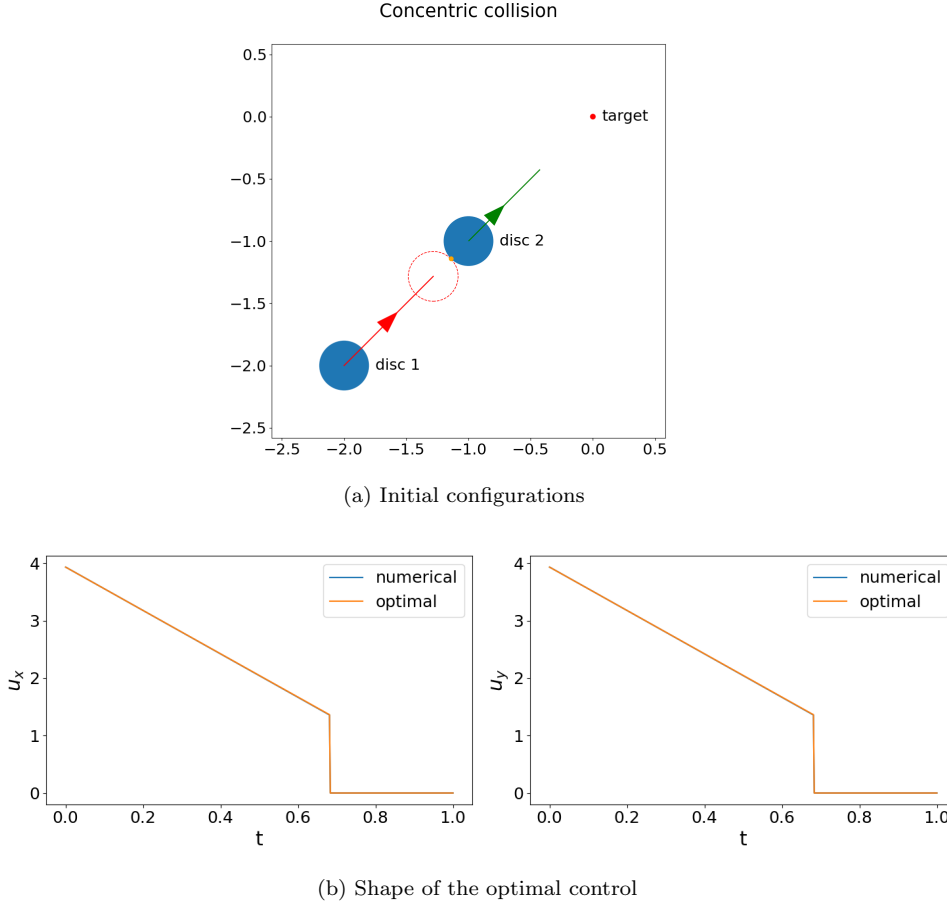


FIG. 5.1. Illustration of the concentric collision in Section 5.1. (a) Initial state: The initial locations of discs are the blue discs. The red line and green line are optimal trajectories of disc 1 and disc 2, respectively. The dashed red circle is the before-collision position of disc 1. The orange point is the collision point. (b) The numerical optimal control and the analytical optimal control, $\mathbf{u} = [u_x, u_y]$.

In Figure 5.5, we show the change of cost, $\|H_u\|_2$ and $\|\mathbf{u} - \mathbf{u}^{opt}\|_2$. We see that a few hundred iterations are sufficient for convergence. We notice that linear convergence is also observed in terms of the convergence indicator $\|H_u\|_2$.

We also demonstrate the convergence to the analytical solution as N increases. Asymptotic first-order accuracy is observed for this case; see Figure 5.6.

5.3. Multiple collisions. In this example, we test our algorithm in the case where multiple collisions are needed to achieve optimality. We add a wall that can be viewed as a rigid body with an infinitely large mass. There are three possible collisions in this system; inter-disc, the wall with disc 1 and the wall with disc 2. A natural way to model this system is to independently model the collision, *i.e.* the detection and jump functions, of each possible colliding pair of rigid bodies. Let us discuss how we can consolidate these collision models into the formulation presented in Section 2. We shall assume that these collisions are isolated, *i.e.* at most one collision occurs at a time.

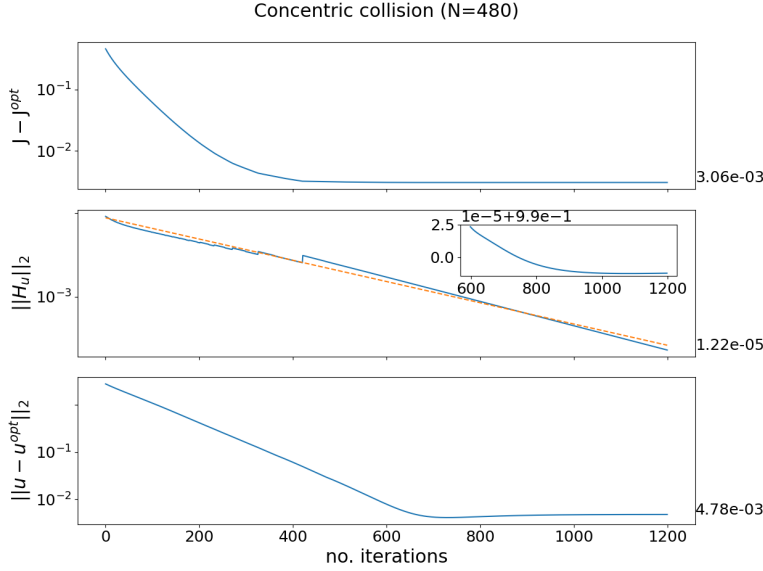


FIG. 5.2. The example of concentric collision in Section 5.1: the convergence of the iterative algorithm. The annotations on the right are the final values of the corresponding curves. The common x axis denotes the number of iterations spent in the Algorithm 1. Top: the difference between the analytical optimal objective and the numerical solutions. Middle: the L^2 semi-norm of the derivative of the Hamiltonian with respect to control \mathbf{u} . The dashed line is the result of the regression in the form $\mu\sigma^k$ (this is the linear regression after taking the logarithm. k is the number of iterations, μ, σ are positive regression parameters). The inset plot is the ratio $\|H_u^{k+1}\|_2 / \|H_u^k\|_2$ versus the number of iterations. It suggests that the rate of linear convergence is approximately 0.99. Bottom: the difference between the analytical optimal control and the numerical solutions in terms of the L^2 semi-norm.

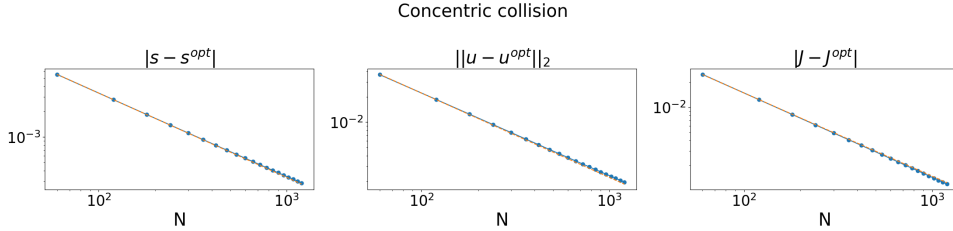
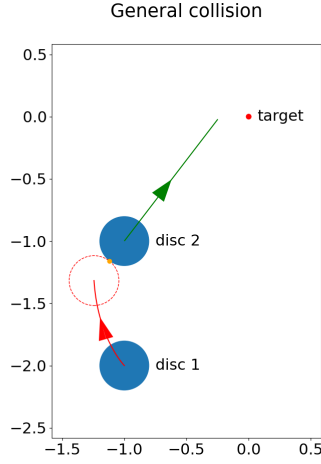
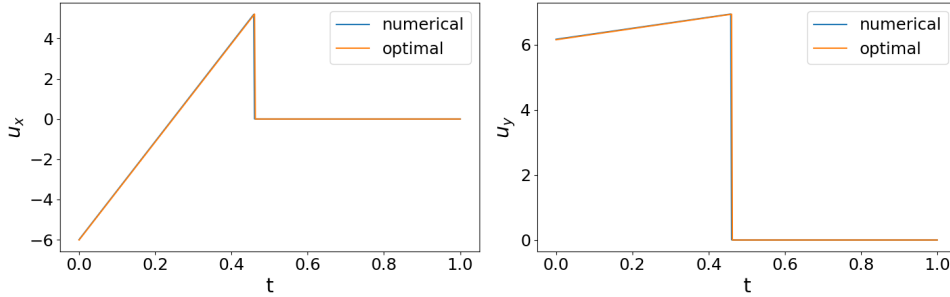


FIG. 5.3. The example of concentric collision in Section 5.1: convergence to the analytical solution when the number of time intervals N tends to infinity. The dashed orange lines are straight lines obtained from the least square regression on the data with model σ/N and parameter σ . Left: Difference between the simulated collision times and the analytical optimal collision time. Middle: Difference between the numerical and analytical solutions for the optimal controls in terms of the L^2 semi-norm. Right: Difference between the simulated total costs and the analytical solution.

In eq. (2.3), we assume that ψ is a positive scalar function. In general, one can introduce a vector-valued detection function $\boldsymbol{\psi}^* = [\psi_1, \dots, \psi_{n_c}]^T : \mathbb{R}^m \rightarrow \mathbb{R}^{n_c}$, where n_c is the number of possible colliding rigid body pairs. Each coordinate ψ_i^* corresponds to the collision detection of a rigid body pair. There are also n_c associated jump functions $\mathbf{g}_1^*, \dots, \mathbf{g}_{n_c}^*$. We assume ψ_i^* and \mathbf{g}_i^* are smooth.



(a) Initial configurations



(b) Shape of the optimal control

FIG. 5.4. *Illustration of the general situation of two discs in Section 5.2. (a) Initial state: The initial locations of the discs are the blue discs. The red and green lines are the optimal trajectories of disc 1 and disc 2, respectively. The dashed red circle is the before-collision position of disc 1. The orange point is the collision point. (b) The numerical and the analytical solutions for the optimal control, $\mathbf{u} = [u_x, u_y]$.*

The vector-valued formulation can be converted to the scalar-valued formulation if collisions are isolated. To be specific, we let $K_i = \{\mathbf{x} : \psi_i^*(\mathbf{x}) = 0\}$, $i = 1, \dots, n_c$ and $B(\mathbf{x}, \delta)$ be the open ball with radius δ centered at \mathbf{x} . The domain of interest is given by

$$\mathcal{X} = \left\{ \mathbf{x} : \begin{array}{l} \exists \delta > 0, i \in \{1, \dots, n_c\} \text{ such that} \\ B(\mathbf{x}, \delta) \cap K_i \neq \emptyset, B(\mathbf{x}, \delta) \cap K_j = \emptyset \text{ for } j \neq i \end{array} \right\}.$$

One can think of this set as follows. We cover the isolated collision states, the union of all jumping manifolds K_i subtracting their pairwise intersections, by open balls intersecting precisely one of those manifolds. According to the definition, for any $\mathbf{x} \in \mathcal{X}$, we can define the unique active index $i(\mathbf{x})$ such that the only possible collision

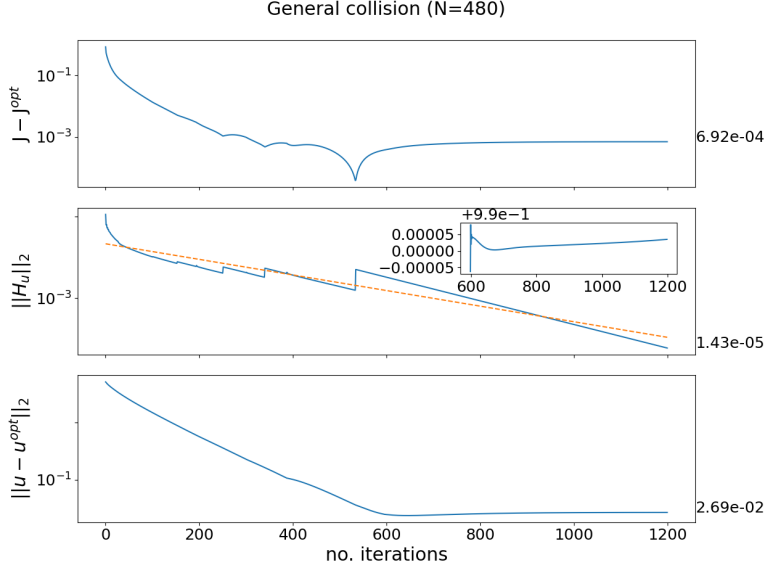


FIG. 5.5. The example of general situation of two discs in Section 5.2: the convergence of the iterative algorithm. The annotations on the right are the final values of the corresponding curves. The common x axis is the number of iterations spent in the Algorithm 1. Top: the difference between the analytical optimal objective and the numerical solutions. Middle: the L^2 semi-norm of the derivative of the Hamiltonian with respect to the control u . The dashed line is the result of the regression in the form $\mu\sigma^k$ (this is the linear regression after taking the logarithm. k is the number of iterations, μ, σ are positive regression parameters). The inset plot is the ratio $\|H_u^{k+1}\|_2 / \|H_u^k\|_2$ versus number of iterations. Bottom: the difference between the analytical optimal control and the numerical solutions in terms of the L^2 semi-norm.

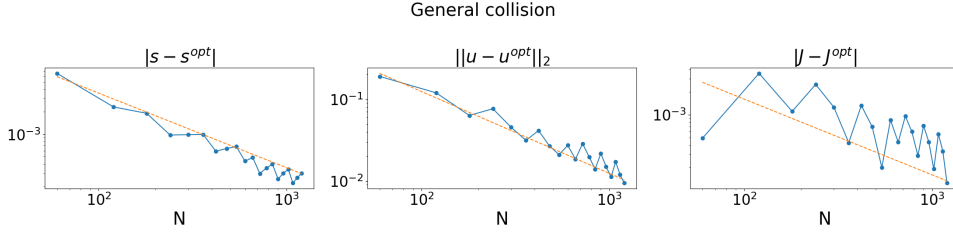


FIG. 5.6. The example of general situation of two discs in Section 5.2: convergence to the analytical solution when the number of time intervals N tends to infinity. The dashed orange lines are straight lines obtained from the least square regression on the data with model σ/N and parameter σ . Left: Difference between the simulated collision times and the analytical optimal collision time. Middle: Difference between the numerical and analytical solutions for the optimal controls in terms of L^2 semi-norm. Right: Difference between the simulated total costs and the optimal analytical solution.

in the neighborhood of \mathbf{x} is on $K_{i(\mathbf{x})}$. We then define, for $\mathbf{x} \in \mathcal{X}$,

$$\psi(\mathbf{x}) = \psi_{i(\mathbf{x})}^*(\mathbf{x}), \quad (5.14a)$$

$$\mathbf{g}(\mathbf{x}) = \mathbf{g}_{i(\mathbf{x})}^*(\mathbf{x}). \quad (5.14b)$$

ψ and \mathbf{g} are smooth in \mathcal{X} since for every $\mathbf{x} \in \mathcal{X}$, $i(\mathbf{x})$ is constant in a ball containing

\mathbf{x} .

We denote the inter-disc collision detection function and jump function defined early in Section 5 as ψ_0, g_0 . The wall is represented by a hyperplane, *i.e.* a straight line in 2D, whose distance to the origin O is b . We denote the normal vector of the wall by \mathbf{n}_w such that $\mathbf{n}_w \cdot OP > 0$ for any point P on the wall. Without loss of generality, we assume the two discs are on the same side of the wall as the origin O , which means the distance from disc i to the wall, $b - \mathbf{x}_{q_i} \cdot \mathbf{n}_w - r_i$, are positive. The distance will decrease if $\mathbf{x}_{v_i} \cdot \mathbf{n}_w > 0$, *i.e.* the velocity of disc i projected to the wall normal is positive. The collision detection function of the wall to disc i can be defined as,

$$\psi_i(\mathbf{x}) = \begin{cases} b - \mathbf{x}_{q_i} \cdot \mathbf{n}_w - r_i & \text{if } \mathbf{n}_w \cdot \mathbf{x}_{v_i} > 0 \\ 1 & \text{elsewhere} \end{cases}.$$

The corresponding jump function \mathbf{g}_i will only change the velocity of disc i as

$$[\mathbf{g}_i(\mathbf{x})]_{v_i} = \mathbf{x}_{v_i} - 2(\mathbf{x}_{v_i} \cdot \mathbf{n}_w)\mathbf{n}_w,$$

while all the other components of $\mathbf{g}_i(\mathbf{x})$ remain the same as \mathbf{x} .

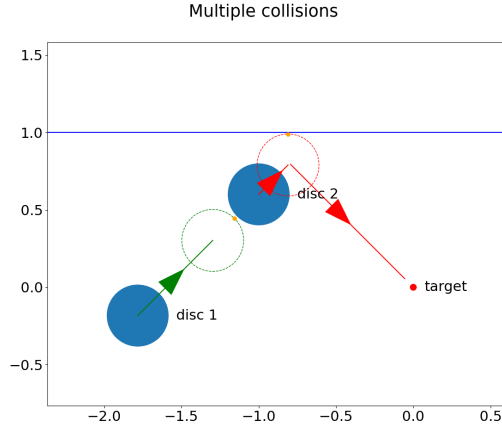
We will be focusing on isolated collisions in this example. Actually, we further assume that there is a gap $\beta > 0$ such that there is at most only one collision in every time interval of length smaller than β . In numerical computation, we can go through the prediction of collision time for every $\psi_i, i = 0, 1, 2$ and let the active index be the one on which the prediction is smaller than Δt , if there is. There will be at most one such index if N , the number of time discretization, is greater than T/β (might be multiplied by a factor if taking into account the error in estimating collision times).

We take the initial state as $\mathbf{q}_1 = [-\frac{3}{2} - \frac{\sqrt{2}}{5}, \frac{1}{10} - \frac{\sqrt{2}}{5}]^T, \mathbf{q}_2 = [-1, \frac{3}{5}]^T, \mathbf{v}_1 = \mathbf{v}_2 = [0, 0]^T$ and $\epsilon = 0.01, T = 1$. The wall, whose normal vector is $[0, 1]^T$, is placed at a distance of 1 to the origin. See Figure 5.7a for an illustration. In this setup, we control disc 1 to collide with disc 2 in the way that disc 2 will approach the target with the help of wall collision. Analytical solution for the optimal control can also be obtained, see Section A.

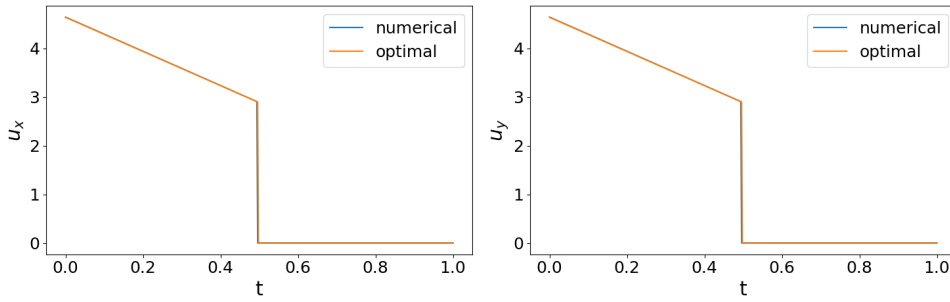
We discretize the dynamics into 480 steps, *i.e.* $N = 480$ and run the Algorithm 1 with the relaxation parameter $\alpha = 0.01$. The initial control is the constant control pointing disc 2 from disc 1 with magnitude $3\sqrt{2}$, *i.e.* $[3, 3]^T$. The numerical result is shown and compared to the analytical one in Figure 5.7b. Again linear convergence is observed, and a few hundred iterations are enough for the algorithm to converge, see Figure 5.8.

As is depicted in Figure 5.9, our optimal numerical control is approaching the analytical solution as Δt approaches zero and the collision times also converge to the analytical ones. We also note that the order of accuracy is still first order. It does not degrade with more collisions.

5.4. Comparison to HMP-MAS. In [43], given the number of switching times, the author proposed to solve the optimal control in multiple autonomous switchings system based on the hybrid maximum principle (HMP-MAS) by alternating between (1) solving for optimal controls in the sub-domains divided by guessed switching time and switching states; (2) computing gradients and updating the guesses by gradient descent. The method has been extended to autonomous hybrid dynamical systems on manifolds [50, 51]. Recently, it has been extended to the autonomous



(a) Initial configurations



(b) Shape of the optimal control

FIG. 5.7. Illustration of the multiple collisions in Section 5.3. (a) Initial state: The initial locations of discs are the blue discs. The green and red lines are optimal trajectories of disc 1 and disc 2, respectively. The dashed green circle is the position of disc 1 when disc 1 collides with disc 2. The dashed red circle is the position of disc 2 when disc 2 collides with the wall. The orange points are the collision points. The blue line represents the wall. (b) The numerical optimal control and the analytical optimal control, $\mathbf{u} = [\mathbf{u}_x, \mathbf{u}_y]$.

hybrid dynamical systems with both state jumps and switches in dynamics in [35]. We adapt this method to the dynamical systems discussed in this paper.

To be specific, we assume that there will be one collision for the optimal control. Starting from a reasonable guess that the collision happens at $t = s$ and at state \mathbf{x}_s^- , we solve two standard optimal control problems: find the minimal cost control that shoots (s, \mathbf{x}_s^-) from $(0, \mathbf{x}_0)$ and find the optimal control that minimizing the running cost and terminal cost starting from \mathbf{x}_s^+ at $t = s$. Then, one can compute the gradient of the total cost with respect to s and \mathbf{x}_s^- and then update them by gradient descent. The constraint $\phi(\mathbf{x}_s^-) = 0$ is enforced as a penalty added to the total costs.

The overall performance of this algorithm is comparable to our algorithm, exhibiting a similar convergence curve and error. However, one needs to prescribe the correct number of collisions beforehand for this method. We run the multiple collisions experiment (section 5.3) starting from an initial trajectory with three collisions (see Figure 5.10). Our algorithm converges to the optimal control with two collisions without any modifications. In contrast, HMP-MAS cannot converge to the optimal

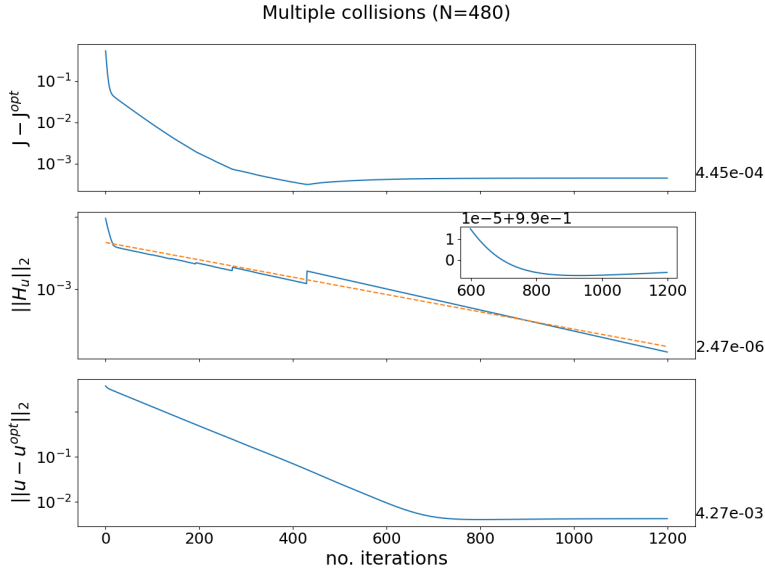


FIG. 5.8. The example of multiple collisions in Section 5.3: the convergence of the iterative algorithm. The annotations on the right are the final values of the corresponding curves. The common x axis is the number of iterations spent in the Algorithm 1. Top: the difference between the analytical optimal objective and the numerical solutions. Middle: the L^2 semi-norm of the derivative of the Hamiltonian with respect to the control \mathbf{u} . The dashed line is the result of the regression in the form $\mu\sigma^k$ (this is the linear regression after taking the logarithm. k is the number of iterations, μ, σ are positive regression parameters). The inset plot is the ratio $\|H_u^{k+1}\|/\|H_u^k\|$ versus the number of iterations. Bottom: the difference between the analytical optimal control and the numerical solutions in terms of the L^2 semi-norm.

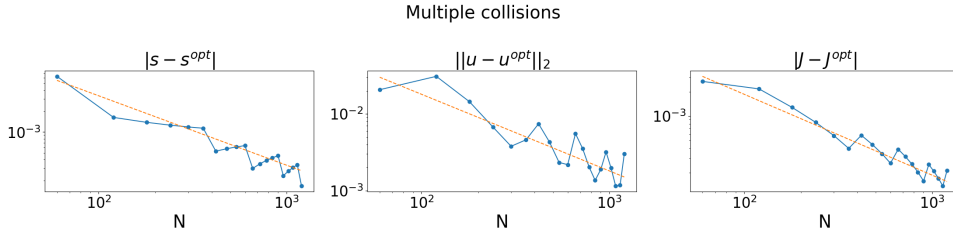


FIG. 5.9. The example of multiple collisions in Section 5.3: convergence to the analytical solution when the number of time intervals N tends to infinity. The dashed orange lines are straight lines obtained by the least square regression on the data with model σ/N and parameter σ . Left: Difference between the simulated collision times and the analytical optimal collision time. Middle: Difference between the numerical and analytical solutions for the optimal controls in terms of L^2 semi-norm. Right: Difference between the simulated total costs and the optimal analytical solution.

solution starting from such an initialization.

5.5. Comparison to a direct method. In this subsection, we compare the Algorithm 1 with a gradient descent algorithm, which is applied to the following

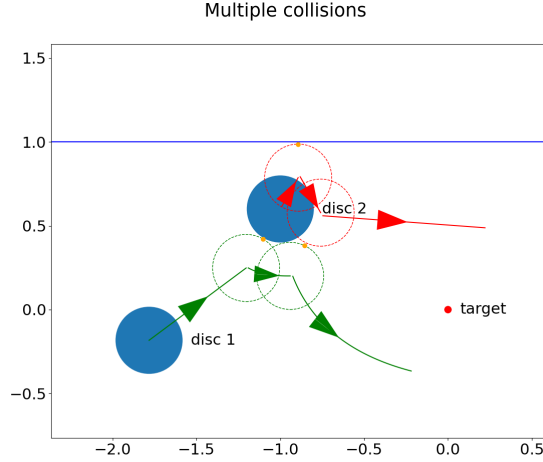


FIG. 5.10. Illustration of the trajectories under a control that results in three collisions. The green and red lines with arrows are trajectories of disc 1 and disc 2, respectively. Dashed green circles and red circles are snapshots of disc 1 and disc 2 when collisions occur, respectively. The orange points are collision points. See Section 5.4.

discretized problem

$$\underset{u_0, \dots, u_{N-1}}{\text{minimize}} \quad \phi(\mathbf{x}_N) + \sum_{i=0}^{N-1} L(\mathbf{x}_i, \mathbf{u}_i) \Delta t, \quad (5.15a)$$

$$\text{subject to} \quad \text{eq. (4.4)}. \quad (5.15b)$$

The discrete dynamics is implemented in PyTorch [38] with gradients with respect to the controls $\mathbf{u}_0, \dots, \mathbf{u}_{N-1}$ been calculated by auto-differentiation.

The learning rate is chosen to be compatible with the Algorithm 1. For the examples considered in this paper, the continuous version of the control update step in Algorithm 1, *i.e.* eq. (4.2), can be rewritten as

$$\mathbf{u}^{k+1} = (1 - \alpha)\mathbf{u}^k + \alpha\mathbf{u}_* = \mathbf{u}^k - \frac{\alpha}{2\epsilon} H_u(\mathbf{x}^k, \boldsymbol{\lambda}^k, \mathbf{u}^k),$$

recalling the minimizer \mathbf{u}_* in eq. (5.10) and H_u in eq. (5.11). Therefore, we set the learning rate to $\frac{\alpha N}{2\epsilon}$, where the factor N is multiplied to compensate the integration step size Δt since the discrete gradient has an additional time step factor Δt compared to the continuous counterpart.¹ We note that selecting a consistent learning rate is only for the purpose of comparison. As can be seen in Figure 5.11, the learning curves of these two methods overlap at the beginning of the iteration. Further changes of the learning rate and more training iterations will not lead to a reduction of the error of the solution in the direct method.

We have compared the performance of the Algorithm 1 and the direct method at $N = 480$ on all three examples considered before, and the comparison is shown

¹We take the functional $\mathcal{S}(v) = \int_0^T v(t)^2 dt$ as an example to explain why discretization introduces the factor Δt in the gradient. Here v is a continuous square-integrable function. The Fréchet functional derivative of $\mathcal{S}(v)$ in L^2 is $S'(v) = 2v$. If we take the discrete approximation of the integral as $\tilde{S}(v_0, \dots, v_{N-1}) = \sum_{i=0}^{N-1} v_i^2 \Delta t$, where v_i are values at t_i , the function $\tilde{S} : \mathbb{R}^N \rightarrow \mathbb{R}$ has gradient $\nabla \tilde{S}(v_0, \dots, v_{N-1}) = 2\Delta t(v_0, \dots, v_{N-1})$.

HMP versus Direct (N=480)

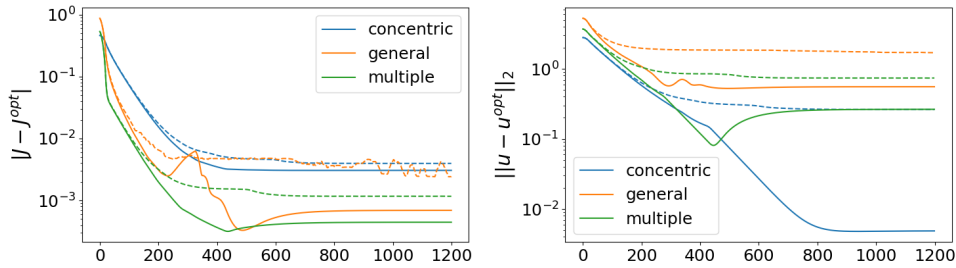


FIG. 5.11. The comparison between HMP (Algorithm 1) and the direct method over all three experiments; the concentric collision (section 5.1), the general situation (section 5.2) and the multiple collisions (section 5.3). Solid lines are data from the Algorithm 1. Dashed lines are data from the direct method; Different colors correspond to different experiments, see legends in the figure. Left: Difference between the simulated total costs and the optimal analytical total costs. Right: Difference between the numerical controls and analytical optimal controls in terms of L^2 semi-norm. See Section 5.5

in Figure 5.11. We find that our HMP-based algorithm always performs much better than the direct method; the numerical solution of the optimal control and the corresponding total cost of the Algorithm 1 are much closer to their analytical ones.

The convergence behavior as $N \rightarrow \infty$ is also compared, see Figures in 5.12. As seen from the figure, the direct method also produces reasonable solutions in terms of the total costs but does not converge well; the errors to the optimal analytical controls measured in L^2 semi-norm show no signs of convergence as N increases. Similar behavior has been observed in the collision times. The direct method produces comparable results regarding the total costs in the concentric collision example and multiple collisions example but still fails to converge in the general situation example.

Despite the fact that their gradients are related, the HMP algorithm and the gradient descent algorithm are still very different. Numerically, the difference can be seen in Figures 5.11 and 5.12. Conceptually, for general forms of the dynamics and cost functional, the update direction in the HMP algorithm based on the stronger minimization conditions (eq. (3.6)) is not parallel to the gradient direction. As pointed out in [48, 23], the gradient of the discrete problem might be incorrect (in the sense that it does not converge to that of the continuous problem). In some cases (like the examples considered in this paper) where the minimization direction coincides with the gradient direction, due to the discontinuities, the numerical approximation of the Fréchet derivatives H_u (of the HMP algorithm, see Remark 3 and eq. (4.14)) are different from the gradients of the discrete problems (of the direct method, see eq. (5.15)). Another point worth noting is that in the HMP algorithm, we can stabilize the numerical computations of H_u (e.g. eqs. (4.8) and (4.9) in the discretization of the backward dynamics) from the continuous point of view. As discussed in Section 4, this is of critical importance for the dynamics with discontinuities. In contrast, it is unclear how to adopt similar stabilization techniques to the direct method.

5.6. Comparison to deep reinforcement learning. Deep reinforcement learning has demonstrated its ability in many complex tasks [32, 31, 46, 47, 33]. In this section, we reformulate the optimal control problem considered in this paper into

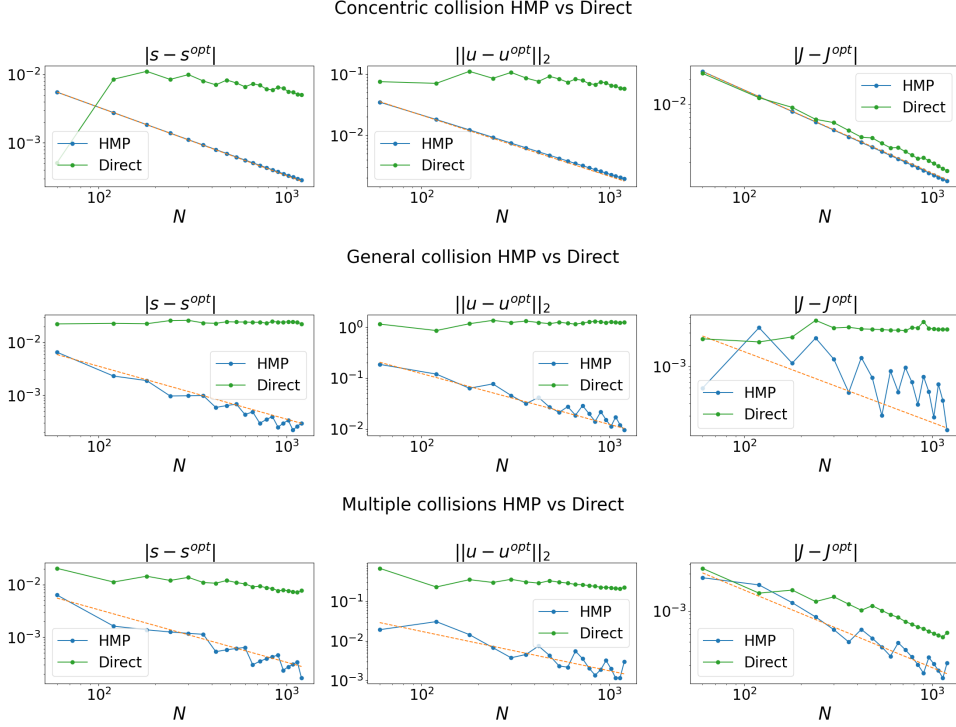


FIG. 5.12. *Convergence to the analytical solution when N increases. The dashed orange lines are straight lines obtained by the least square regression on the results of the Algorithm 1 with model σ/N and parameter σ . Top: The concentric collision example (section 5.1). Middle: The general situation example (section 5.2). Bottom: The multiple collisions example (section 5.3). Left: Difference between the simulated collision times and the analytical optimal collision times. Middle: Difference between the numerical controls and the analytical optimal controls in terms of L^2 semi-norm. Right: Difference between the simulated total costs and the optimal analytical solutions. See Section 5.5*

a reinforcement learning problem and test the performance of a modern advanced deep reinforcement learning algorithm: Proximal Policy Optimization (PPO) algorithm [42].

We take the example of the concentric collision in section 5.1. The observation space is the time-state space $\mathbb{R}^9 = (t, \mathbf{x})$, $t \in [0, T]$, $\mathbf{x} \in \mathbb{R}^8$. The action space is the two-dimensional control whose components are scaled to $[-1, 1]$,

$$\bar{\mathbf{u}} = \frac{\mathbf{u} + 5}{10}.$$

Here we assume that each component of the actual control takes values in $[-5, 5]$. We use Stable-Baselines 3 [41] to implement the PPO algorithm. We use two-layer neural networks for the actor and critic networks; each layer has 64 neurons. Each episode in the training consists of $N = 60$ time steps.

As discussed previously, due to the control cost, the randomly initialized policy network will quickly converge to zero. It is necessary to encourage exploration by using a warm-up step. This is done by setting the running cost L to zero in the early

training stage. We train the warm-up stage for 3000 episodes. The policy network starts converging after a series of actions that triggers a collision is exploited. See the inset of the right subfigure of Figure 5.13. Afterwards, we restore the running cost defined in eq. (5.8) and train another 80000 episodes.

The convergence history of the rewards and the profile of the best control policy are shown in Figure 5.13. We observe that the best policy is obtained at around $3000 + 60000$ episodes. After that, the control network starts converging to zero. The best policy found is still far from optimal. The optimal total cost found by the PPO algorithm is 1.617140, which is 15.80% suboptimal to the optimal cost of 1.396542. Note that the optimal cost found by the Algorithm 1 is 1.421552.

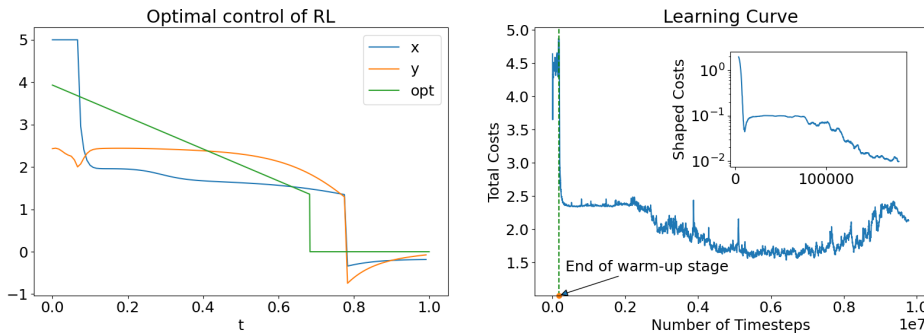


FIG. 5.13. The performance of the deep reinforcement learning algorithm (PPO) described in section 5.6 on the example of concentric collision. Left: the optimal control found by the PPO. Curves labelled with x, y are the x, y components of the control, respectively. The green curve labeled with “opt” is the analytical optimal control (its x, y components are the same). Right: the evolution of the total cost versus training steps. The modified costs (with running costs dropped) are plotted for the warm-up stage in the inset plot at log scale.

6. Summary and future work. This paper presents a numerical algorithm for finding the optimal control of dynamical systems with autonomous state jumps. We consider the dynamical system that models the collisional rigid body dynamics, a critical component of many practical applications. We put forward several techniques to address the numerical issues brought by the discontinuities. We test the proposed algorithm on several examples in which the optimal controls drive the discs to collide in order to achieve the lowest total cost. Comparisons to HMP-MAS, direct method, and deep reinforcement learning demonstrate the superiority of the proposed algorithm in terms of accuracy, efficiency, and flexibility. Implemented with the forward-Euler scheme, the algorithm shows linear convergence with respect to the iteration steps and asymptotic first-order accuracy in terms of time discretization.

The proposed method can be extended in a few directions.

General shapes. In general, there are more complex-shaped rigid bodies. These shapes introduce additional challenges in computing both the functions and their derivatives of the collision detection functions ψ and the jump functions g . Besides, angular quantities such as orientation, angular velocity, and torques are often needed to describe the system. These quantities can still be fully characterized under the formulation in Section 2.

Contact dynamics. Contacts are another essential feature in many applications. They can be viewed as continuous collisions in certain time intervals. Examples

range from robotic arm, *e.g.* fetch environments (the FetchPush and FetchSlide [39]) to quadrupeds [24] and humanoids [53, 28]. Instead of modeling their dynamics by continuous collisions, we may formulate them as autonomous switching dynamical systems. When entering the contact surface and under an applied impulse, the right-hand side function f changes discontinuously. The dynamical system can be formulated as in Section 2 and a corresponding HMP can be derived. A successive approximation type algorithm can be constructed similar to that in Section 4.

Frictional dynamics. Frictional force is critical in many applications, from simple models like the hopper [19] and swimmer [16], to complex models like the quadrupeds [24] and humanoid [53, 28]. The frictional forces are always present together with contacts/collisions. Frictions introduce extra discontinuity and nonlinearity to the dynamical system, in addition to collisions and contacts. It can be viewed as a set-valued function consisting of two modes; the following formula is a one-dimensional example,

$$f(v) \in \begin{cases} \{-\mu N\} & \text{if } v > 0 \\ \{\mu N\} & \text{if } v < 0, \\ [-\mu N, \mu N] & \text{if } v = 0 \end{cases},$$

where μ is the frictional coefficient, N is the normal contact force, and v is the relative velocity.

Frictional dynamics can also be described in the framework of switching systems. The presence of frictions adds additional dependency of the discontinuities on the state, *i.e.* the relative velocity. In addition, it is usually a source of nonlinearity since friction takes value in a cone determined by the magnitude of the normal contact force, which is a more complex function of the state.

A. Analytical optimal controls. The common parameters are summarized in Table 5.1. In the examples considered, the optimal control should drive disc 1 to collide with disc 2 so that disc 2 is close to the origin at the terminal time $T = 1$. Recall that we always assign zero initial velocity to disc 2. Let us assume that disc 1 collides with disc 2 with velocity \mathbf{v}' at the collision time s . The after collision velocity of disc 2 is $\mathbf{v} = (\mathbf{v}' \cdot \mathbf{n})\mathbf{n}$, see Section 5. The displacement of disc 1 before collision is a linear function of \mathbf{n} ,

$$\begin{aligned} \mathbf{d} &= \mathbf{q}_1(s) - \mathbf{q}_1(0) = \mathbf{q}_2(s) - (r_1 + r_2)\mathbf{n} - \mathbf{q}_1(0) \\ &= \mathbf{q}_2(0) - \mathbf{q}_1(0) - (r_1 + r_2)\mathbf{n}. \end{aligned} \tag{A.1}$$

Here $\mathbf{q}_1, \mathbf{q}_2$ are the positions of disc 1, disc 2, respectively. Given the collision time s , the collision velocity \mathbf{v}' and the contact normal \mathbf{n} , the optimal control \mathbf{u} before collision can be obtained by solving,

$$\underset{\mathbf{u}}{\text{minimize}} \quad \int_0^s L(\mathbf{x}, \mathbf{u}) dt \tag{A.2a}$$

$$\text{subject to} \quad \int_0^s \mathbf{u}(t) dt = \mathbf{v}', \tag{A.2b}$$

$$\int_0^s (s-t)\mathbf{u}(t) dt = \mathbf{d}. \tag{A.2c}$$

The optimal control after collision is identically zero. In the case $L(\mathbf{x}, \mathbf{u}) = \epsilon|\mathbf{u}|^2$, the optimal control before collision is

$$\mathbf{u}(t) = \frac{6\mathbf{d}}{s^2} - \frac{2\mathbf{v}'}{s} + \left(\frac{6\mathbf{v}'}{s^2} - \frac{12\mathbf{d}}{s^3}\right)t. \quad (\text{A.3})$$

Then, the total cost is

$$\begin{aligned} & \phi(\mathbf{x}(T)) + \int_0^T L(\mathbf{x}, \mathbf{u}) dt \\ &= |\mathbf{q}_2(s) + (T-s)(\mathbf{v}' \cdot \mathbf{n})\mathbf{n}|^2 + \epsilon\left(\frac{12}{s^3}|\mathbf{d}|^2 + \frac{4}{s}|\mathbf{v}'|^2 - \frac{12}{s^2}\mathbf{v}' \cdot \mathbf{d}\right). \end{aligned} \quad (\text{A.4})$$

Recall that \mathbf{d} is a linear function of \mathbf{n} , $\mathbf{q}_2(s) = \mathbf{q}_2(0)$, the objective A.4 depends only on s , \mathbf{v}' and \mathbf{n} .

Example 5.1. In the configuration described in Section 5.1 where concentric collision is preferred, the optimal $\mathbf{n} = \frac{1}{\sqrt{2}}(1, 1)$, and the optimal \mathbf{v} takes the form $\mathbf{v} = (v_c, v_c)$, $v_c \in \mathbb{R}$. Then the total cost A.4 is quadratic in v_c whose optimal value can be analytically solved as a function of s . Finally, we turn the total cost into a rational function of s , whose minimizer in $(0, T)$ can be computed using an analytical solution to machine accuracy.

Example 5.2. In the the general situation described in Section 5.2, one cannot solve the optimal contact normal vector easily. Note that the total cost (A.4) is quadratic in \mathbf{v}' , we can first minimize it with respect to \mathbf{v}' . To this end, we set the gradient of the total cost with respect to \mathbf{v}' to zero to have

$$\mathbf{v}' \cdot \mathbf{n}^\perp = \frac{3\mathbf{d} \cdot \mathbf{n}^\perp}{2s}, \quad \mathbf{v}' \cdot \mathbf{n} = -\frac{s^2(T-s)\mathbf{q}_2(0) \cdot \mathbf{n} - 6\epsilon\mathbf{d} \cdot \mathbf{n}}{4\epsilon s + s^2(T-s)^2}, \quad (\text{A.5})$$

where $\mathbf{n}^\perp = \begin{pmatrix} 0 & -1 \\ 1 & 0 \end{pmatrix} \mathbf{n}$ is obtained by rotating \mathbf{n} 90 degrees. Then, the total cost (A.4) is rational in s and is a fourth order polynomial in the coordinates of \mathbf{n} . The constraints are $|\mathbf{n}|^2 = 1$ and $s \in (0, T)$. Therefore, minimization of the total cost can be solved to machine accuracy using an analytical solution.

Example 5.3. In the multiple collisions example described in Section 5.3, the velocity of a disc with velocity $\mathbf{v} = (\mathbf{v}_x, \mathbf{v}_y)$ becomes $(\mathbf{v}_x, -\mathbf{v}_y)$ after a collision with the wall $y = b$. Let us denote the velocity of disc 2 after the collision with disc 1 by $\mathbf{v} = (\mathbf{v}_x, \mathbf{v}_y)$. It takes time $(b - r_2 - \mathbf{q}_{2,y}(s))/\mathbf{v}_y$ for disc 2 to collide with the wall, where $\mathbf{q}_{2,y}(s)$ is the y coordinate of the position of disc 2 at time s . Thus the terminal cost is

$$\begin{aligned} & |\mathbf{q}_{2,x}(s) + \mathbf{v}_x(T-s)|^2 + \left| (b - r_2) - \mathbf{v}_y\left(T - s - \frac{b - r_2 - \mathbf{q}_{2,y}(s)}{\mathbf{v}_y}\right) \right|^2 \\ &= |\mathbf{q}_{2,x}(s) + \mathbf{v}_x(T-s)|^2 + |\mathbf{q}_{2,y}(s) + (T-s)\mathbf{v}_y - 2(b - r_2)|^2, \end{aligned}$$

namely, the square distance to the point $(0, 2(b - r_2))$ as if there is no wall. The optimal control for this case can be computed using the same procedure as in the previous examples.

REFERENCES

- [1] Vladimir V Aleksandrov. On the accumulation of perturbations in the linear systems with two coordinates. *Vestnik MGU*, 3:67–76, 1968.
- [2] Michael Athans and Peter L. Falb. *Optimal control. An introduction to the theory and its applications*. McGraw-Hill Book Co., New York-Toronto, Ont.-London, 1966.
- [3] Vadim Azhmyakov, Sid Ahmed Attia, and Jörg Raisch. On the maximum principle for impulsive hybrid systems. In *Hybrid systems: computation and control*, volume 4981 of *Lecture Notes in Comput. Sci.*, pages 30–42, Berlin, Heidelberg, 2008. Springer, Berlin.
- [4] Vadim Azhmyakov, Vladimir G. Boltyanski, and Alexander S. Poznyak. Optimal control of impulsive hybrid systems. *Nonlinear Analysis: Hybrid Systems*, 2(4):1089–1097, 2008.
- [5] Vadim Azhmyakov and Jörg Raisch. A gradient-based approach to a class of hybrid optimal control problems. *IFAC Proceedings Volumes*, 39(5):89–94, 2006. 2nd IFAC Conference on Analysis and Design of Hybrid Systems.
- [6] Richard Bellman. Dynamic programming. *Science*, 153(3731):34–37, 1966.
- [7] Thomas J Böhme and Benjamin Frank. *Hybrid Systems, Optimal Control and Hybrid Vehicles*. Springer International Publishing AG, Switzerland, 2017.
- [8] Michael S. Branicky, Vivek S. Borkar, and Sanjoy K. Mitter. A unified framework for hybrid control. In *Proceedings of 1994 33rd IEEE Conference on Decision and Control*, volume 4, pages 4228–4234 vol.4, 1994.
- [9] Michael S. Branicky, Vivek S. Borkar, and Sanjoy K. Mitter. A unified framework for hybrid control: model and optimal control theory. *IEEE Trans. Automat. Control*, 43(1):31–45, 1998.
- [10] Mirko Brentari, Sofia Urbina, Denis Arzelier, Christophe Louembet, and Luca Zaccarian. A hybrid control framework for impulsive control of satellite rendezvous. *IEEE Transactions on Control Systems Technology*, 27(4):1537–1551, 2019.
- [11] B Brogliato, AA ten Dam, L Paoli, F Ge´not, and M Abadie. Numerical simulation of finite dimensional multibody nonsmooth mechanical systems. *Applied Mechanics Reviews*, 55(2):107–150, 04 2002.
- [12] Sam Burden, Humberto Gonzalez, Ram Vasudevan, Ruzena Bajcsy, and S. Shankar Sastry. Numerical integration of hybrid dynamical systems via domain relaxation. In *2011 50th IEEE Conference on Decision and Control and European Control Conference*, pages 3958–3965, 2011.
- [13] Peter E. Caines, F. H. Clarke, X. Liu, and R. B. Vinter. A maximum principle for hybrid optimal control problems with pathwise state constraints. In *Proceedings of the 45th IEEE Conference on Decision and Control*, pages 4821–4825, 2006.
- [14] M. B. Carver. Efficient integration over discontinuities in ordinary differential equation simulations. *Math. Comput. Simulation*, 20(3):190–196, 1978.
- [15] Felix L. Chernousko and Alexey A. Lyubushin. Method of successive approximations for solution of optimal control problems. *Optimal Control Appl. Methods*, 3(2):101–114, 1982.
- [16] Rémi Coulom. *Reinforcement learning using neural networks, with applications to motor control*. PhD thesis, Institut National Polytechnique de Grenoble-INPG, 2002.
- [17] Andrei V Dmitruk and Alexander M Kaganovich. The hybrid maximum principle is a consequence of Pontryagin maximum principle. *Systems Control Lett.*, 57(11):964–970, 2008.
- [18] Brian J. Driessen and Nader Sadegh. Minimum-time control of systems with Coulomb friction: near global optima via mixed integer linear programming. *Optimal Control Applications & Methods*, 22(2):51–62, 2001.
- [19] Tom Erez, Yuval Tassa, and Emanuel Todorov. Infinite-horizon model predictive control for periodic tasks with contacts. In *Robotics: Science and Systems*, 2011.
- [20] Joel M. Esposito, Vijay Kumar, and George J. Pappas. Accurate event detection for simulating hybrid systems. In Maria Domenica Di Benedetto and Alberto Sangiovanni-Vincentelli, editors, *Hybrid Systems: Computation and Control*, pages 204–217, Berlin, Heidelberg, 2001. Springer Berlin Heidelberg.
- [21] Mauro Garavello and Benedetto Piccoli. Hybrid necessary principle. *SIAM J. Control Optim.*, 43(5):1867–1887, 2005.
- [22] Zhi-hong Guan, David J. Hill, and Jing Yao. A hybrid impulsive and switching control strategy for synchronization of nonlinear systems and application to chua’s chaotic circuit. *International Journal of Bifurcation and Chaos*, 16(01):229–238, 2006.
- [23] Yuanming Hu, Luke Anderson, Tzu-Mao Li, Qi Sun, Nathan Carr, Jonathan Ragan-Kelley, and Frédo Durand. DiffTaichi: Differentiable programming for physical simulation. *ICLR*, 2020.
- [24] Marco Hutter, Christian Gehring, Dominic Jud, Andreas Lauber, C. Dario Bellicoso, Vassilios Tsounis, Jemin Hwangbo, Karen Bodie, Peter Fankhauser, Michael Bloesch, Remo Diethelm, Samuel Bachmann, Amir Melzer, and Mark Hoepflinger. Anymal - a highly

- mobile and dynamic quadrupedal robot. In *2016 IEEE/RSJ International Conference on Intelligent Robots and Systems (IROS)*, pages 38–44, 2016.
- [25] Aleksandr Davidovich Ioffe and Vladimir Mihajlović Tihomirov. *Theory of extremal problems*. North-Holland Publishing Company, Amsterdam, 2009.
- [26] David H. Jacobson and David Q. Mayne. *Differential dynamic programming*. Modern Analytic and Computational Methods in Science and Mathematics, No. 24. American Elsevier Publishing Co., Inc., New York, 1970.
- [27] Namwook Kim, Sukwon Cha, and Hwei Peng. Optimal control of hybrid electric vehicles based on pontryagin’s minimum principle. *IEEE Transactions on Control Systems Technology*, 19(5):1279–1287, 2011.
- [28] Scott Kuindersma, Robin Deits, Maurice Fallon, Andrés Valenzuela, Hongkai Dai, Frank Permenter, Twan Koolen, Pat Marion, and Russ Tedrake. Optimization-based locomotion planning, estimation, and control design for the atlas humanoid robot. *Autonomous robots*, 40(3):429–455, 2016.
- [29] Qianxiao Li, Long Chen, Cheng Tai, and Weinan E. Maximum principle based algorithms for deep learning. *Journal of Machine Learning Research*, 18:Paper No. 165, 29, 2017.
- [30] Weiwei Li. and Emanuel Todorov. Iterative linear quadratic regulator design for nonlinear biological movement systems. In *Proceedings of the First International Conference on Informatics in Control, Automation and Robotics - Volume 1: ICINCO*, pages 222–229, Portugal, 2004. INSTICC, SciTePress.
- [31] Timothy P. Lillicrap, Jonathan J. Hunt, Alexander Pritzel, Nicolas Heess, Tom Erez, Yuval Tassa, David Silver, and Daan Wierstra. Continuous control with deep reinforcement learning. In Yoshua Bengio and Yann LeCun, editors, *4th International Conference on Learning Representations, ICLR 2016, San Juan, Puerto Rico, May 2-4, 2016, Conference Track Proceedings*, 2016.
- [32] Volodymyr Mnih, Koray Kavukcuoglu, David Silver, Andrei A. Rusu, Joel Veness, Marc G. Bellemare, Alex Graves, Martin Riedmiller, Andreas K. Fidjeland, Georg Ostrovski, Stig Petersen, Charles Beattie, Amir Sadik, Ioannis Antonoglou, Helen King, Dharshan Kumaran, Daan Wierstra, Shane Legg, and Demis Hassabis. Human-level control through deep reinforcement learning. *Nature*, 518(7540):529–533, Feb 2015.
- [33] Matej Moravčík, Martin Schmid, Neil Burch, Viliam Lisý, Dustin Morrill, Nolan Bard, Trevor Davis, Kevin Waugh, Michael Johanson, and Michael Bowling. Deepstack: Expert-level artificial intelligence in heads-up no-limit poker. *Science*, 356(6337):508–513, 2017.
- [34] Michael Neunert, Farbod Farshidian, Alexander W. Winkler, and Jonas Buchli. Trajectory optimization through contacts and automatic gait discovery for quadrupeds. *IEEE Robotics and Automation Letters*, 2(3):1502–1509, 2017.
- [35] Ali Pakniyat and Peter E. Caines. On the hybrid minimum principle: the Hamiltonian and adjoint boundary conditions. *IEEE Trans. Automat. Control*, 66(3):1246–1253, 2021.
- [36] Laetitia Paoli and Michelle Schatzman. A numerical scheme for impact problems. I. The one-dimensional case. *SIAM J. Numer. Anal.*, 40(2):702–733, 2002.
- [37] Laetitia Paoli and Michelle Schatzman. A numerical scheme for impact problems. II. The multidimensional case. *SIAM J. Numer. Anal.*, 40(2):734–768, 2002.
- [38] Adam Paszke, Sam Gross, Soumith Chintala, Gregory Chanan, Edward Yang, Zachary DeVito, Zeming Lin, Alban Desmaison, Luca Antiga, and Adam Lerer. Automatic differentiation in PyTorch. Technical report, 2017.
- [39] Matthias Plappert, Marcin Andrychowicz, Alex Ray, Bob McGrew, Bowen Baker, Glenn Powell, Jonas Schneider, Josh Tobin, Maciek Chociej, Peter Welinder, Vikash Kumar, and Wojciech Zaremba. Multi-goal reinforcement learning: Challenging robotics environments and request for research, 2018.
- [40] Lev Semenovich Pontryagin. *Mathematical theory of optimal processes*. CRC press, Switzerland, 1987.
- [41] Antonin Raffin, Ashley Hill, Adam Gleave, Anssi Kanervisto, Maximilian Ernestus, and Noah Dormann. Stable-baselines3: Reliable reinforcement learning implementations. *Journal of Machine Learning Research*, 22(268):1–8, 2021.
- [42] John Schulman, Filip Wolski, Prafulla Dhariwal, Alec Radford, and Oleg Klimov. Proximal policy optimization algorithms. *arXiv preprint arXiv:1707.06347*, 2017.
- [43] Mohammad Shahid Shaikh and Peter E. Caines. On the hybrid optimal control problem: Theory and algorithms. *IEEE Transactions on Automatic Control*, 52(9):1587–1603, 2007.
- [44] L. F. Shampine, I. Gladwell, and R. W. Brankin. Reliable solution of special event location problems for ODEs. *ACM Trans. Math. Software*, 17(1):11–25, 1991.
- [45] Athanasios Sideris and James E. Bobrow. An efficient sequential linear quadratic algorithm for solving nonlinear optimal control problems. *IEEE Trans. Automat. Control*, 50(12):2043–

- 2047, 2005.
- [46] David Silver, Aja Huang, Chris J. Maddison, Arthur Guez, Laurent Sifre, George van den Driessche, Julian Schrittwieser, Ioannis Antonoglou, Veda Panneershelvam, Marc Lanctot, Sander Dieleman, Dominik Grewe, John Nham, Nal Kalchbrenner, Ilya Sutskever, Timothy Lillicrap, Madeleine Leach, Koray Kavukcuoglu, Thore Graepel, and Demis Hassabis. Mastering the game of go with deep neural networks and tree search. *Nature*, 529(7587):484–489, Jan 2016.
 - [47] David Silver, Julian Schrittwieser, Karen Simonyan, Ioannis Antonoglou, Aja Huang, Arthur Guez, Thomas Hubert, Lucas Baker, Matthew Lai, Adrian Bolton, Yutian Chen, Timothy Lillicrap, Fan Hui, Laurent Sifre, George van den Driessche, Thore Graepel, and Demis Hassabis. Mastering the game of go without human knowledge. *Nature*, 550(7676):354–359, Oct 2017.
 - [48] David E. Stewart and Mihai Anitescu. Optimal control of systems with discontinuous differential equations. *Numer. Math.*, 114(4):653–695, 2010.
 - [49] Héctor J. Sussmann. A maximum principle for hybrid optimal control problems. In *Proceedings of the 38th IEEE Conference on Decision and Control (Cat. No.99CH36304)*, volume 1, pages 425–430 vol.1, 1999.
 - [50] Farzin Taringoo and Peter E. Caines. Gradient-geodesic HMP algorithms for the optimization of hybrid systems based on the geometry of switching manifolds. In *49th IEEE Conference on Decision and Control (CDC)*, pages 1534–1539, 2010.
 - [51] Farzin Taringoo and Peter E. Caines. Gradient geodesic and newton geodesic HMP algorithms for the optimization of hybrid systems. *Annual Reviews in Control*, 35(2):187–198, 2011.
 - [52] Farzin Taringoo and Peter E. Caines. On the extension of the hybrid minimum principle to riemannian manifolds. In *2011 50th IEEE Conference on Decision and Control and European Control Conference*, pages 3301–3306, 2011.
 - [53] Yuval Tassa, Tom Erez, and Emanuel Todorov. Synthesis and stabilization of complex behaviors through online trajectory optimization. In *2012 IEEE/RSJ International Conference on Intelligent Robots and Systems*, pages 4906–4913, 2012.
 - [54] Kok Lay Teo, Bin Li, Changjun Yu, and Volker Rehbock. *Applied and computational optimal control—a control parametrization approach*, volume 171 of *Springer Optimization and Its Applications*. Springer, Cham, Switzerland, 2021.
 - [55] Emanuel Todorov and Weiwei Li. A generalized iterative lqg method for locally-optimal feedback control of constrained nonlinear stochastic systems. In *Proceedings of the 2005, American Control Conference, 2005.*, pages 300–306 vol. 1, 2005.
 - [56] Yu. M. Volin and G. M. Ostrovskii. A maximum principle for discontinuous systems and its application to problems with phase constraints. *Radiophysics and Quantum Electronics*, 12(11):1253–1263, 1969.